

A PRECISION DETERMINATION OF THE K X-RAY FLUORESCENCE YIELD
OF ARSENIC FROM THE RADIOACTIVE DECAY OF SOLID Se^{75} SOURCES

A THESIS

Presented to

The Faculty of the Division of Graduate
Studies and Research

By

William Mahlon Chew

In Partial Fulfillment
of the Requirements for the Degree
Master of Science in Chemistry

Georgia Institute of Technology

March, 1972

A PRECISION DETERMINATION OF THE K X-RAY FLUORESCENCE YIELD
OF ARSENIC FROM THE RADIOACTIVE DECAY OF SOLID Se^{75} SOURCES

Approved:

[Handwritten signature]

Chairman:

[Handwritten signature]

Date approved by Chairman: MAR - 2 1972

ACKNOWLEDGMENTS

It is with great pleasure that I recognize the following persons who have aided me in this investigation.

I wish to express my most sincere appreciation to my thesis advisor, Professor R. W. Fink, without whose support and guidance this work could not have been accomplished. I would also wish to thank Professor T. F. Moran and Professor E. T. Patronis, who not only kindly agreed to serve on the reading committee, but who also provided inspired instruction in several of their courses.

A great deal of credit is due to Dr. J. C. McGeorge, who served as my technical advisor in a postdoctoral capacity and who also carefully reviewed this manuscript and suggested many improvements. It has been a pleasure working with him both as an advisor and a friend. Dr. J. S. Hansen and Dr. W. D. Schmidt-ott have provided much insight through many fruitful discussions of technical aspects of this work. Dr. H. D. Genz provided invaluable assistance in the theoretical determination of the quantity P_K .

I am greatly indebted to Mr. R. D. Smith, who constructed the source holder for the multiwire proportional

counter and in general helped maintain and service the proportional counter and vacuum system. I also wish to thank Mr. D. Nix who aided me in the determination of the emission rates of the Co^{57} sources.

I also wish to thank my parents for instilling within me a desire for knowledge and the perseverance to overcome obstacles to personal goals. I especially wish to thank my wife, Amy, who has supported and encouraged me during this entire project.

TABLE OF CONTENTS

	Page
ACKNOWLEDGMENTS	ii
LIST OF TABLES	vi
LIST OF ILLUSTRATIONS	vii
SUMMARY	viii
Chapter	
I. INTRODUCTION	1
1.1 The Purpose of the Investigation	1
1.2 The Experimental Method and Properties of Se^{75}	3
1.3 Previous Work at $Z=33$	4
II. THE DETERMINATION OF THE PRODUCT $P_K \omega_K \epsilon_K$	7
2.1 Preparation of the Se^{75} Source	7
2.2 Apparatus and Electronic System	7
2.3 Experimental Procedure	12
2.4 Evaluation of the Product $P_K \omega_K \epsilon_K$	16
III. THE DETERMINATION OF THE DETECTION EFFICIENCY ϵ_K	21
3.1 Detection Efficiency Curves for the Si(Li) X-Ray Detector	21
3.2 Absolute K X-Ray Emission Rate of Se^{75}	24
3.2.1 Development of the Method	24
3.2.2 Apparatus and Electronic System	33
3.2.3 Procedure	37
3.3 Evaluation of ϵ_K	39
IV. THE EVALUATION OF ω_K	44
4.1 Calculation of the Quantity P_K	44
4.2 Final Results and Evaluation of Errors	48
V. Discussion	52
5.1 Comparison with Theory	52

TABLE OF CONTENTS (Concluded)

Chapter	Page
5.2 Comparison of the Gaseous and Solid Methods in Determining ω_K in the Region $25 \leq Z \leq 43$	55
5.3 Suggestions for Further Research . .	58
APPENDICES	
A. EFFICIENCY VS PRESSURE COMPUTER PROGRAM .	61
B. SPECTRA STRIPPING COMPUTER PROGRAM . . .	64
REFERENCES	69

LIST OF TABLES

Table		Page
1.	Schedule of Experimental Runs	13
2.	Experimental Quantities Used to Evaluate the Product $P_K \omega_K \epsilon_K$	17
3.	Photon Emissions Used in the Efficiency Curves	22
4.	Effects of the Conical Photon Beam	28
5.	Data Used to Evaluate ϵ_K	40
6.	Theoretical Quantities Used in the Evaluation of P_K	46
7.	The Errors in the Evaluation of ω_K	50
8.	Theoretical Values for ω_K at $Z=33$	53

LIST OF ILLUSTRATIONS

Figure	Page
1. Experimental values of ω_K in the Region $25 \leq Z \leq 43$	2
2. Decay Scheme of Se^{75}	5
3. Block Diagram for $P_K \omega_K \epsilon_K$	9
4. Effects of Ringing	15
5. Efficiency Curves for Si(Li) Detector	23
6. Comparison of Experimental and Calculated Efficiency-Pressure Curves	30
7. Count-Rate - Voltage Curves	31
8. Source Holder Arrangement for the Proportional Counter	35
9. Block Diagram for the Standardization of Sources	36
10. Efficiency Curve with the Se^{75} Point Included	43
11. Theoretical Curves of ω_K , $25 \leq Z \leq 43$	53

SUMMARY

There appear to be two classes of experimental values for K-shell fluorescence yields, ω_K , in the low-to-middle-Z region; (1) measurements using gaseous radioactive sources or fluorescent excitation of nonradioactive gaseous targets, and (2) measurements utilizing solid radioactive sources or solid nonradioactive targets. The first class gives somewhat higher values of ω_K and are presumed to be the more accurate. This thesis contains three contributions. (1) A precision measurement of $\omega_K = 0.589 \pm 0.027$ for $Z=33$ (arsenic) has been made through the use of a solid radioactive Se^{75} source. The errors consist of a 2σ statistical error added linearly to the systematic error. (2) The value is in good agreement with $\omega_K = 0.587$ for the same Z obtained by Pahor, Kodre, and Moljk, who utilized the method of fluorescent excitation of nonradioactive gaseous AsH_3 in a multiwire proportional counter. Therefore, there is no difference between the two types of measurements, at least for $Z=33$. (3) During the course of the present investigation, a new method of calibrating the absolute emission rates of low energy (<30 keV) photon emitting radioactive sources was developed.

CHAPTER I

INTRODUCTION

1.1 The Purpose of the Investigation

In the region of $25 \leq Z \leq 43$, there appear to be two classes of experimental results for the K-shell fluorescence yields, ω_K ; (1) measurements obtained by techniques involving the use of gaseous radioactive sources or nonradioactive targets in proportional counters, and (2) measurements obtained by techniques involving the use of solid sources or targets. The "most reliable" experimental values of ω_K , which are listed in a forthcoming review paper¹, are shown plotted against atomic number Z in Fig. 1, along with the semiempirical curve¹ fitted to these values. Those experimental points which lie on, or below, the semiempirical curve, Fig. 1, were obtained through the use of solid radioactive sources or by fluorescent excitation of solid targets. On the other hand, all but one of the experimental points which lie above the semiempirical curve, Fig. 1, were obtained through fluorescent excitation of nonradioactive gaseous targets, or by means of internal gaseous radioactive sources in proportional counters.

The gaseous methods have been generally thought to have smaller uncertainty, since they are not subject to self-absorption or absorption due to materials between the

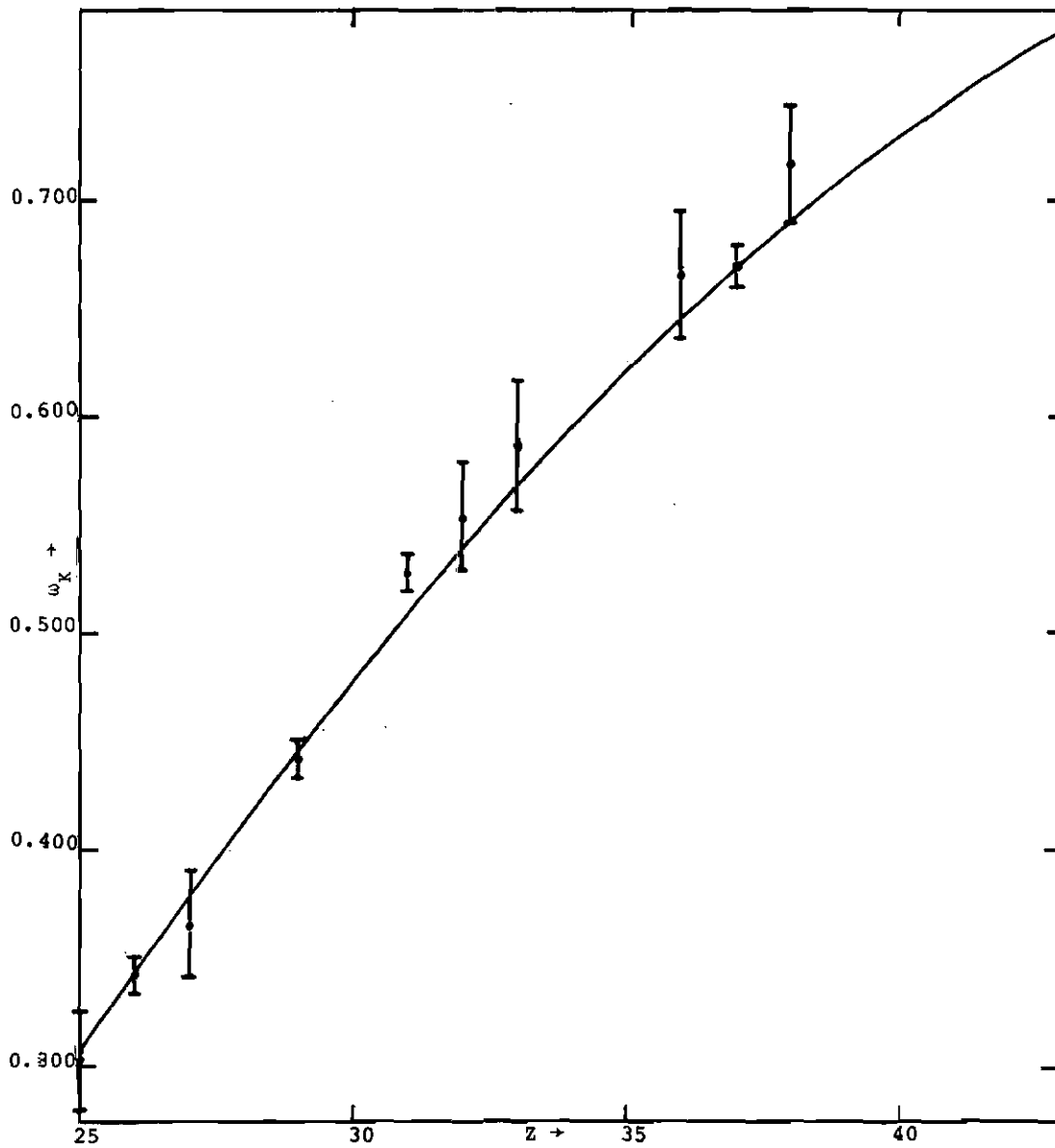


Fig. 1. Experimental values of ω_K in the Region $25 \leq z \leq 43$.
(taken from Bambynek et al. ref. 1)

source and the detector. A principal objective of this thesis is to demonstrate at $Z=33$ whether a careful measurement with an ultrathin solid radioactive source confirms the trend established by the gaseous techniques, since the two methods have completely different systematic errors. In addition, during the course of this investigation, a new method of calibration of low-energy (<30 keV) radioactive photon sources was developed.

1.2 The Experimental Method and Properties of Se^{75}

The present method^{2,3}, using a solid radioactive source of Se^{75} , is based on a precision determination of the product $P_K \omega_K \epsilon_K$, where P_K is the probability of K-capture to a level in the daughter nucleus, ω_K is the K-shell fluorescence yield, defined as the ratio of total K x-ray emission to the number of K-shell vacancies, and ϵ_K is the overall efficiency for detection of the K x rays. From the $P_K \omega_K \epsilon_K$ product, the K-shell fluorescence yield ω_K is evaluated by taking P_K from experimentally-confirmed theoretical calculations (see Sect. 4.1), and ϵ_K is measured experimentally (see Chept. III).

The ideal radioactive source for the method is one having a decay scheme in which an electron capture branch leads to a level in the daughter nucleus which is not fed by any other transitions and which has a direct transition to the ground state with little internal conversion. The

γ -ray transition is then used to gate the coincident K x-ray spectrum. From these coincidence measurements, the product $P_K \omega_K \epsilon_K$ can be determined by means of the equations set forth in Sect. 2.3 below. In practice, however, there may be "true" coincidences with the "tails" of higher energy γ -rays present, as well as chance coincidences. Corrections must be made for both of these effects. The former correction may be obtained through a coincidence spectrum gated by pulses from a region of the γ -spectrum just above the γ -ray used to gate the main run, and may be taken simultaneously. The chance correction can be obtained from a separate run taken with an extra time delay added to one side of the coincidence counting systems. These corrections are discussed in more detail in Sect. 2.3.

The nuclide Se^{75} decays with a 120.4 ± 0.2 day half life⁴ by electron capture to various levels in As^{75} ($Z=33$). The decay scheme is shown in Fig. 2, and is based on that of Paradellis and Hontzeas⁵, with weak transitions and electron capture branches omitted for clarity. The coincidence measurement is made with the 400.7 keV gamma ray and the ~ 10.5 keV K x-ray group resulting from K-capture to the 400.7 keV level (see Chapt. II).

1.3 Previous Work at Z=33

There are two previous $P_K \omega_K \epsilon_K$ measurements at $Z=33$ using solid radioactive Se^{75} sources. In both cases a

value of ω_K was assumed and P_K was evaluated. Raeside et al.⁶ obtained $P_K \omega_K = 0.462 \pm 0.026$ which implies $\omega_K = 0.527$ if $P_K = 0.876 \pm 0.004$ (discussed in Sect. 4.1). Rao et al.⁷ gave a value of $P_K \omega_K = 0.460 \pm 0.026$ which gives $\omega_K = 0.525$ using the same value for P_K . In both cases, the ω_K values fall far below the semiempirical curve in Fig. 1. This would indicate that the detection efficiencies used in both cases were too large, or thick sources were used resulting in self-absorption, or both.

An early value of $\omega_K \approx 0.53$ obtained through fluorescent excitation of a solid target was determined by Berkey⁸ in 1934. This value also falls below the semiempirical curve in Fig. 1. Pahor, Kodre, and Moljk⁹ have recently obtained $\omega_K = 0.587 \pm 0.003$, by using fluorescent excitation of a gaseous nonradioactive target. In Fig. 1 this value lies slightly above the semiempirical curve, but it is subject to a 5 percent systematic uncertainty owing to the necessity in this method to assume a value for the "K-jump", as discussed in Sect. 5.2.

CHAPTER II

THE DETERMINATION OF THE PRODUCT $P_K \omega_K \epsilon_K$

2.1 Preparation of the Se^{75} Source

The source used in the investigation was made by drop evaporation of 2 μ liters of a solids-free Se^{75} solution obtained from New England Nuclear Corporation. This process was done carefully to keep self-absorption minimal, and the resulting source intensity was about 2 μ Curies in a 4 mm diameter spot which was barely visible.

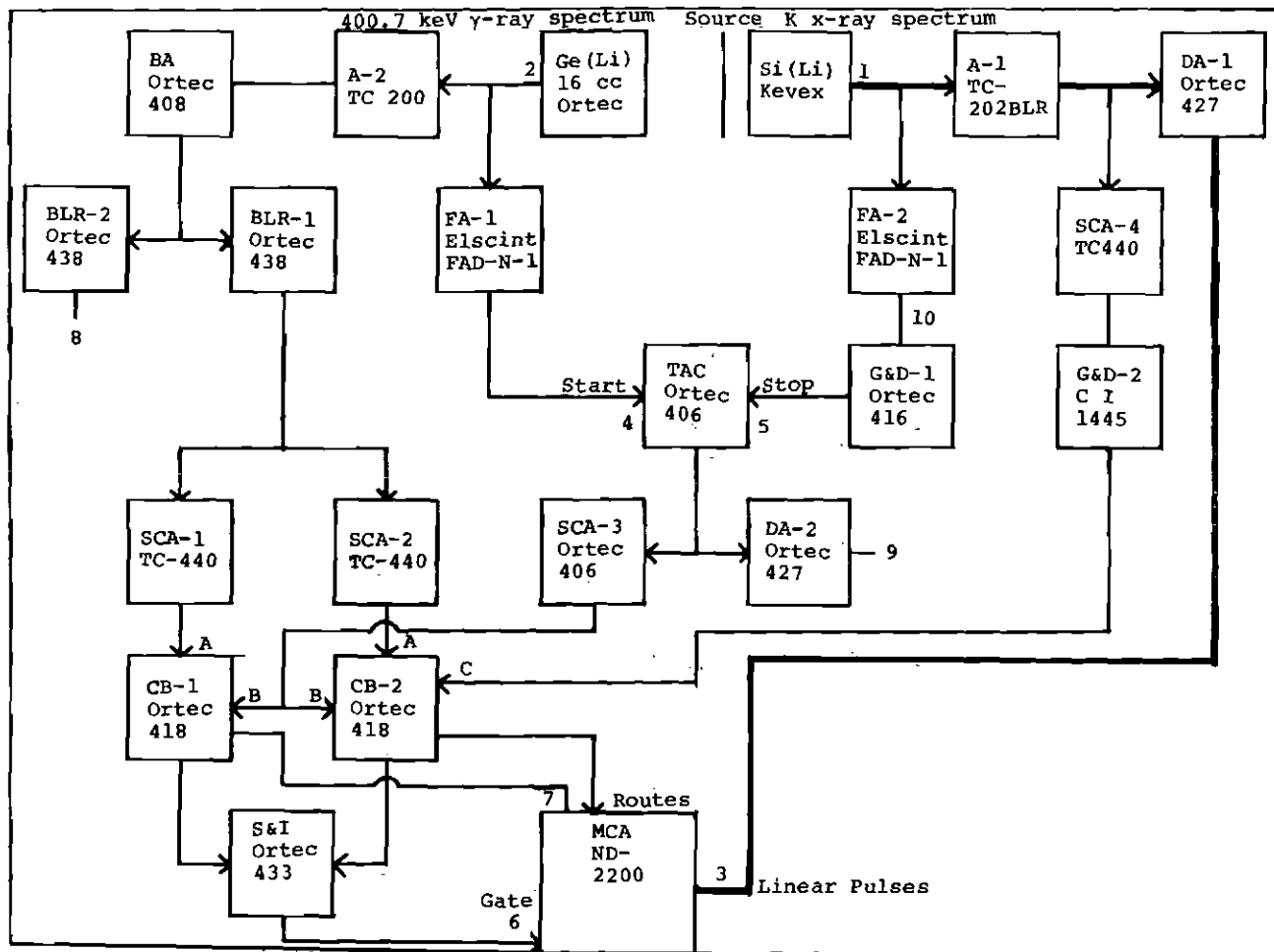
2.2 Apparatus and Electronic System

The electronic system is set up such that two requirements are met before a pulse is stored in the coincident spectrum. The first requirement is that pulses originate in both the gate and the x-ray detectors within a predetermined period of time (called the resolving time 2τ). This is determined in the time, or fast, branch of the coincidence system, and in order to do this accurately, all energy information is destroyed. The second requirement is that the pulse in the gate detector be of a desired energy. This is determined in the linear, or slow, branch of the coincidence system. This measurement, therefore, utilizes a fast-slow coincidence system.

Two semiconductor detectors were placed in 180° coincidence geometry. The first, a lithium-drifted silicon crystal of 6 mm diameter and 3 mm depth, was used to detect arsenic K x rays from the decay of a solid, high-specific-activity Se^{75} radioactive source placed on a source holder attached to the detector housing. The source was approximately 1 cm from the 0.005 cm thick (0.002 inch) beryllium window. The second detector, a 16 cm^3 lithium drifted germanium crystal at about 2.5 cm behind the source, was used to detect gamma photons, and the 400.7 keV γ -ray was used as a gating signal.

The block diagram of the fast-slow coincidence system is shown in Fig. 3. Pulses from the Si(Li) x-ray detector(1) were fed into a linear amplifier(A-1), delayed 3 μsec , and then put into the linear input of a 2048-channel Nuclear Data 2200 series multichannel analyzer(MCA) at point 3.

The output of the Ge(Li) γ -ray detector(2) was fed into a linear amplifier(A-2), and then a biased amplifier(BA) followed by a baseline restorer(BLR-1). This arrangement was used to increase the number of channels in the 400.7 keV γ -ray peak. The window of a single-channel analyzer(SCA-1) was set on a region above the gamma peak, in order to obtain an x-ray spectrum which was in coincidence with the tails of higher energy γ -rays from the Se^{75} source. The output of SCA-1 was fed into a coincidence unit(CB-1) and



Block Diagram for P_{K^0} , E_K , E_K^+ Measurements. The following abbreviations are used:

A - linear amplifier; BA - biased amplifier; DA - delay amplifier; FA - fast amplifier; BLR - baseline restorer; CB - coincidence unit; G&D - gate and delay generator; MCA - multichannel analyzer; SCA - single channel analyzer; TAC - time to amplitude converter; S&I - sum and invert amplifier; Ge(Li) - lithium drifted germanium detector; Si(Li) - lithium drifted silicon detector.

represented the slow branch(A) of the coincidence for the background. The output of the baseline restorer(BLR-1) was also fed into a single-channel analyzer(SCA-2), the window of which was set on the 400.7 keV γ -ray peak. The output of SCA-2 was fed into a coincidence unit(CB-2) and represented the slow branch(A) of the coincidence of the 400.7 keV γ -ray. During the runs, the coincidence circuits demanded both the slow(A) and the fast(B) signals. The output signals from both coincidence units were summed in a sum-invert amplifier(S&I), after which they entered the multichannel analyzer(MCA) at its gating input(6). Routing pulses from the coincidence units also entered the MCA at point 7, in order to determine in which portion of the MCA memory the linear signal was to be stored. One quadrant of the memory held the spectrum in coincidence with γ -rays, and a second quadrant held the background spectrum due to higher energy γ -ray tails.

Pulses from both detectors were fed into fast amplifiers(FA's), which are the first stages of the fast part of the system. The time-to-amplitude converter(TAC) received its start pulse from FA-1 (from the γ -ray detector), and the signals from FA-2 (from the x-ray detector) were delayed by 1 μ sec and used to stop the TAC. The TAC was set on 2 μ sec for maximum pulse-height (5 volts). The resulting time spectrum gave a peak at about 950 nanosec. A third single-channel analyzer(SCA-3) was set on the time

peak. The window of the SCA determined the resolving time, 2τ . The output of SCA-3 constituted the fast coincidence pulse and was supplied to both coincidence units at point B.

To obtain the γ -ray spectrum, self-gated by its own fast and slow pulses, the input of a gate and delay generator (G&D-1) was replaced by a second signal from FA-1. In this manner, the TAC was started and stopped by the same signal originating in the Ge(Li) γ -ray detector. A linear signal from the biased amplifier was fed into a baseline-restorer (BLR-2), the output of which was delayed by a delay amplifier (DA-2) and put into the linear input of the MCA at point 3. In this arrangement, single-channel analyzers SCA-1 and SCA-2 could be set merely by demanding pulse A in the coincidence circuits, or the self-gated γ -ray spectrum could be obtained by demanding pulses A and B.

To obtain the self-gated x-ray spectrum, cables were changed from FA-1 to FA-2, thereby starting and stopping the TAC with the same fast pulse originating from the Si(Li) x-ray detector. A fourth single-channel analyzer (SCA-4) was set on the x-ray spectrum coming from amplifier A-1; the output of SCA-4 was slightly delayed (to give a similar timing arrangement as signal A in the coincidence units) and then fed into coincidence unit-2. The coincidence circuit was then set to demand both pulses B and C. The linear x-ray pulses followed the heavy path shown in Fig. 3.

To obtain a time spectrum, pulses from the TAC (with the cables set as in Fig. 3) were delayed by a delay amplifier(DA-2) and fed into the linear input of the MCA at point 3. The self gated time spectrum was then obtained by demanding only pulse B at one of the coincidence units.

3.2 Experimental Procedure

A schedule of runs is given in Table 1. Before and after each run, self-gated time, 400.7 keV γ -ray, and K x-ray spectra were taken as checks of the system. This was done to assure that no change occurred in the electronics during each run. Two chance runs were taken by moving single-channel analyzer SCA-3 well off the peak of the time spectrum.

When the first chance run was analyzed, it was found that 7.19 percent of the coincidences in the first two runs were due to chance. An estimate of the number of chance coincidences expected was made by use of the following equation and was found to be lower than observed by a factor of 2.

$$C_C = C_\gamma \cdot 2\tau \cdot (C_K/t) \quad (1)$$

Where C_C = the number of K x-ray chance counts in a run;

C_γ = the number of γ -ray (gate openings) in a run;

C_K = the number of singles K x-ray counts in time t ; and

2τ = the resolving time.

Table 1. Schedule of Experimental Runs

Run Number	Duration (hours)	Type of Coincidence Measurement
1	47	(K X-ray)-(400 keV γ -ray)
2	63	(K X-ray)-(400 keV γ -ray)
3	23	Chance
4	62	(K X-ray)-(400 keV γ -ray)
5	19	Chance
6	43	(K X-ray)-(400 keV γ -ray)

This discrepancy was found to arise from double-pulsing due to ringing from fast amplifier FA-2. Careful adjustment of the threshold of the fast amplifier and the placement of a resistor in series with the input of the amplifier eliminated ringing due to K x rays, although higher energy γ -rays still produced ringing.[†] If a resistor large enough to stop the ringing of the γ -rays were placed in series with the input, then the K x rays could not be seen. The effect of the ringing of the γ -rays does not contribute much to the total chance rate, as there would be a two-fold chance involved: first, two γ -rays would have to enter the detectors at the proper time, such that a ringing would stop the TAC within the time interval allowed by the

[†]The effect of the ringing due to an x-ray event is as follows (see Fig. 4). If an x ray is seen in the Si(Li) detector, a series of pulses from the fast amplifier will be produced. If a 400.7 keV γ -ray is seen in the Ge(Li) gate detector after the original delayed x-ray pulse enters the TAC, but before one of the afterpulses arrives, the TAC will produce a spurious pulse. Some of these spurious events will have the correct pulse height to be passed through the SCA into the coincidence unit. This opens the gate to the MCA, because the same γ -ray which starts the TAC will also pass through SCA-2 and be seen by the coincidence unit. The x ray, which started the ringing, would then enter the MCA while the gate is open, because the x-ray is delayed by 3 μ sec. This effectively increases the resolving time 2τ and results in an increased chance coincidence rate.

On the other hand, a true coincidence event (Fig. 4) would not be affected by this phenomenon, since the γ -ray precedes the x ray at the TAC and starts a 2 μ sec sweep. The TAC will not accept another start (γ -ray) pulse until this sweep is completed, which in effect, gives a 2 μ sec paralysis time. The coincident x ray will arrive somewhere during the sweep and determines the height of the output pulse. The TAC will then ignore afterpulses until it completes its sweep, at which time almost all the ringing is stopped.

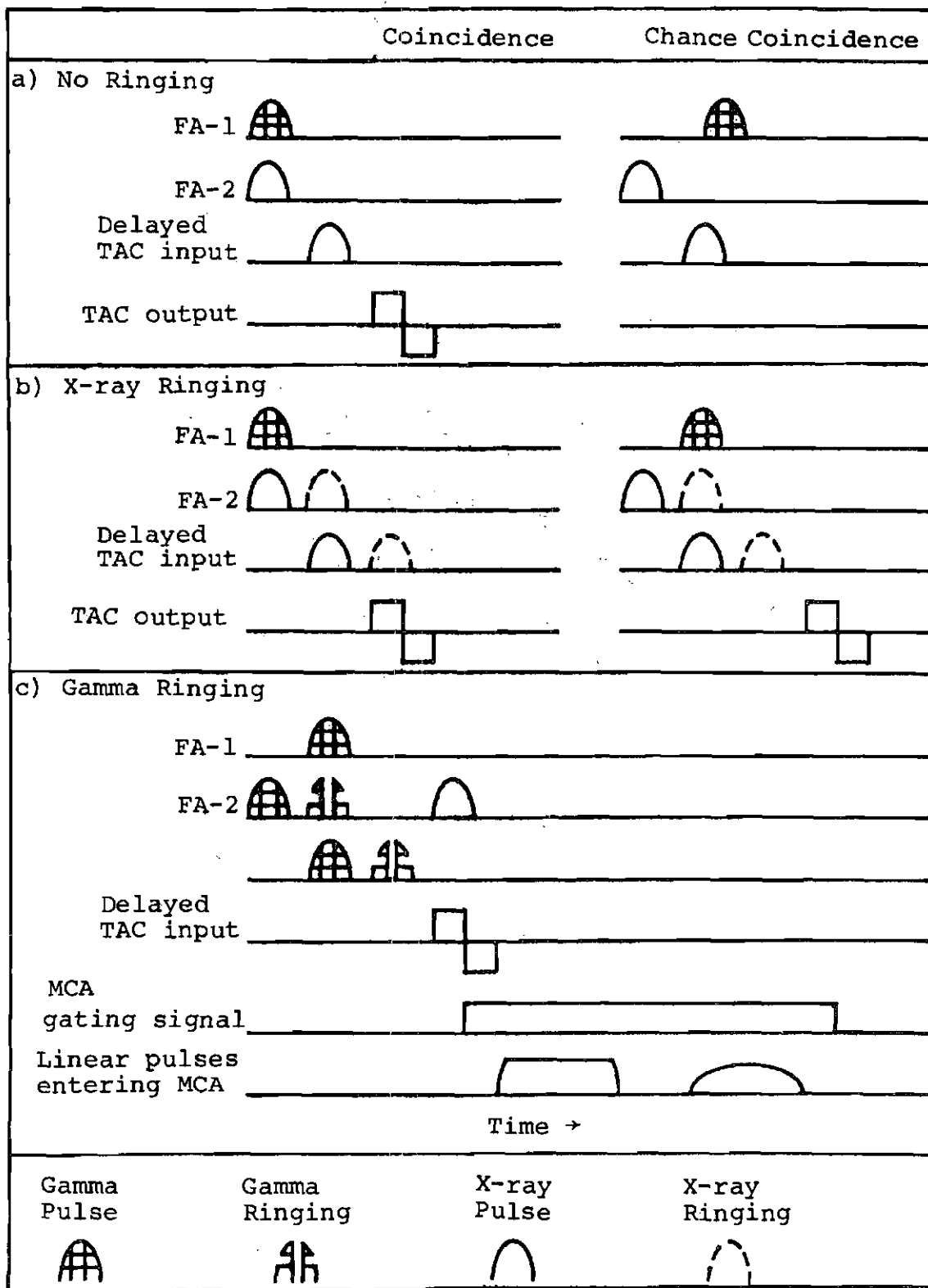


Fig. 4. Effects of Ringing.

single-channel analyzer(SCA-3), and second, an x ray would have to come shortly after the γ -ray in the Si(Li) detector such that it would be seen within the 6 μ sec opening of the coincidence gate to the multichannel analyzer, but not so soon as to produce summing with the γ -ray (see Fig. 4). This effect would at least be an order of magnitude smaller than the effect of the double pulsing due to an x ray event.

Before the fourth run (Table 1), the resolving time was changed to about 210 nanosec by narrowing the window of SCA-3 which was set on the time spectrum. This reduced only the chance coincidence rate, but the coincidence efficiency remained at unity, since the time peak was 140 nanosec wide and therefore remained in the time window of SCA-3. The second chance run gave a 2.26 percent chance rate, as compared with a 2.24 percent chance rate calculated from the data from run 4 (Table 1) using equation 1. Therefore the effects of ringing were essentially negligible for runs 4 and 6 (Table 1).

A series of efficiency runs for the Si(Li) detector were made at both the coincidence geometry (1 cm from the beryllium window) and at a lower, more reproducible, geometry (5 cm). These will be discussed in Sect. 3.1.

2.4 Evaluation of the Product $P_K \omega_K \epsilon_K$

The results of the experiment are given in Table 2. The equation used to obtain these results is as follows:

Table 2. Experimental Quantities Used to Evaluate
the Product $P_K^{\omega_K \epsilon_K}$

Run	$C_K(\gamma)$	$\frac{X}{Y} C_K(>\gamma)$	XPGC	N_γ	$\frac{X}{Y} N_{>\gamma}$	$P_K^{\omega_K \epsilon_K}$
1	36904	389	.000202	13243516	160185	.002589
2	48628	404	.000202	17634012	169873	.002559
4	44300	318	.000059	16883989	158494	.002571
6	30701	201	.000059	11566727	108368	.002603

Final Result: $P_K^{\omega_K \epsilon_K} = 0.00258 \pm 0.000028$

$$P_{K\omega_K\epsilon_K} = \frac{C_K(\gamma) - (x/y)C_K(>\gamma) - XPGC\{N_\gamma - (x/y)N_{>\gamma}\}}{N_\gamma - (x/y)N_{>\gamma}} \quad (2)$$

where $C_K(\gamma)$ is the number of K x-ray counts in coincidence with the 400.7 keV γ -ray; $C_K(>\gamma)$ is the number of K x-ray counts in coincidence with the tails of higher energy γ -rays; N_γ is the number of γ -ray counts, which equals the number of gate openings on the 400.7 keV γ -ray; $N_{>\gamma}$ is the number of gate openings due to the tails of higher energy γ -rays; XPGC is the x ray per gamma chance counting rate which equals $C_K(\gamma)_{\text{chance}}/N_{\gamma \text{ chance}}$; and x/y is the ratio of the gate widths of single channel analyzers SCA-2 and SCA-1 respectively.

This equation is not difficult to derive. The quantity $P_{K\omega_K\epsilon_K}$ is just the ratio of K x rays in true coincidence with 400.7 keV γ -rays to the true number of those γ -rays. The quantity $C_K(\gamma)$ is the experimental number of x ray- γ -ray coincidences, but it includes background due to higher energy γ -rays and also chance coincidences. The background term is just the number of coincidences with coincidence unit CB-1 normalized to the ratio of the window widths of SCA-2 and SCA-1, respectively. The correction term for chance coincidences is just the ratio of x-ray counts per γ -ray obtained from the chance runs multiplied by the number of gate counts of the 400.7 keV γ -rays during a coincidence run. However, this corrects twice for chance

coincidences which are due to the background from higher energy γ -ray tails, so one has to add back this amount.

Equation 2 becomes after simplification:

$$P_{K^{\omega}K^{\epsilon}K} = \frac{C_K(\gamma) - (x/y)C_K(>\gamma)}{N_{\gamma} - (x/y)N_{>\gamma}} - XPGC$$

The final result for $P_{K^{\omega}K^{\epsilon}K}$ is:

$$P_{K^{\omega}K^{\epsilon}K} = 0.00258 \pm 0.000028.$$

The error limits represent a 2σ standard deviation taken from the counting statistics of the individual runs. The 2σ standard deviation from the spread of the results (σ_r) is 0.000039 (or 1.5 percent). The similarity between σ_r and σ_s (the statistical error given with the result) suggests that deviations not due to counting statistics are considerably less than one percent. However, because such deviations may not be entirely negligible as compared with the standard deviation of the mean (± 0.000014 or 0.53 percent), the standard deviation σ_s (1.1 percent) is used as an indication of the error in $P_{K^{\omega}K^{\epsilon}K}$.

One should also notice that there is no trend between the first two coincidence runs and the second two coincidence runs, which indicates that the afterpulsing phenomenon does not contribute significantly to the error when an experimental determination of the chance rate is used. Moreover, the reduction of the resolving time

affects only the chance rate (as predicted). If the true chance rate were affected, the second pair of runs would be smaller than the first pair.

CHAPTER III

THE DETERMINATION OF THE DETECTION EFFICIENCY ϵ_K 3.1 Detection Efficiency Curves for the
Si(Li) X-Ray Detector

A series of spectra from standard Am^{241} and Co^{57} radioactive sources was obtained, in order to determine the detection efficiency curves for the Si(Li) x-ray detector used in the $P_K \omega_K \epsilon_K$ investigation. The efficiency of detecting the K x rays of arsenic is then taken from this curve. The efficiencies obtained for both the coincidence and a lower, more reproducible 5 cm, geometry are given in Table 3 for various energies obtained from the two standards. The two resulting efficiency curves are shown in Fig. 5.

It is obvious from the efficiency curves for this particular detector that there is an unpredictable jump from the 11.9 keV point (Np L_2 x ray from the Am^{241} standard) to the 6.4 keV point (Co^{57} standard). The possible origin of this jump is discussed in Sect. 3.3. Since the energy of the K x rays of arsenic fall in this region, large errors would result in the efficiency for As K x rays if these curves were used. Therefore, it was decided to standardize the Se^{75} source used in the

Table 3. Photon Emissions Used in Efficiency Curves

Standard	Photon	Energy keV	ϵ (Near Geometry) $\times 10^{-3}$	ϵ (Far Geometry) $\times 10^{-4}$
Am^{241}	L_{ℓ} x ray	11.9	4.579 ± 0.058	6.633 ± 0.108
	L_{α} "	13.9	4.452 ± 0.058	6.490 ± 0.036
	L_{β} "	17.8	4.014 ± 0.011	5.909 ± 0.010
	L_{γ} "	20.6	3.467 ± 0.039	3.444 ± 0.060
Co^{57}	K x ray	6.4	5.044 ± 0.026	7.080 ± 0.050
	γ -ray	14.4	4.539 ± 0.064	6.518 ± 0.080

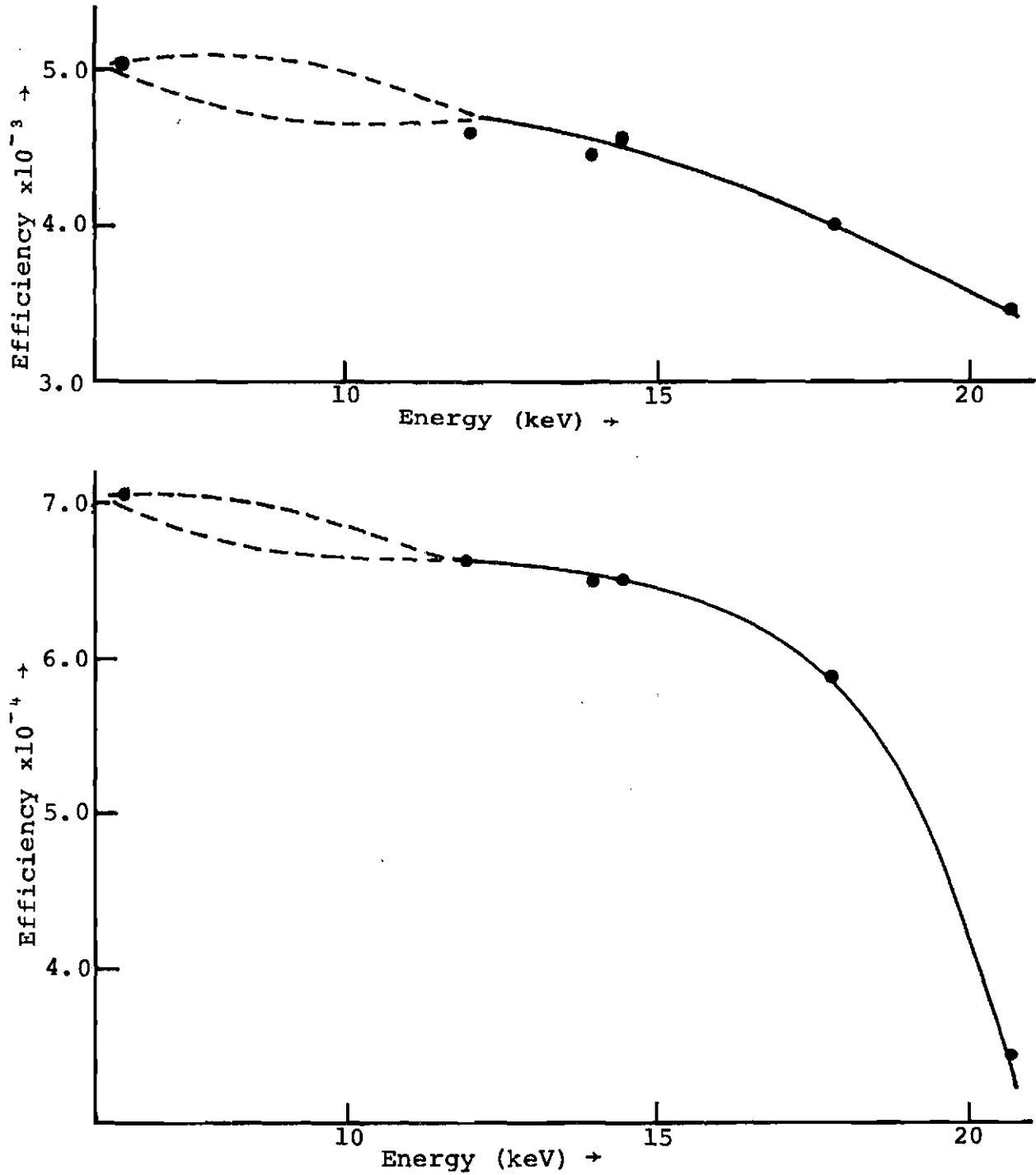


Fig. 5. Efficiency Curves for Si(Li) Detector.

coincidence experiment. One could then use this new standard to obtain the detection efficiency of the x-ray detector.

It should also be noted that the Am^{241} standard, used to find these curves, has since been found to be thick enough to cause substantial self-absorption and self-excitation. Therefore, the accuracy of the efficiency points due to the Am^{241} source is somewhat doubtful.

3.2 Absolute K X-Ray Emission Rate of Se^{75}

3.2.1 Development of the Method. Since standard sources with a suitable photon energy between 6.5 and 14.4 keV are not available, a new method was developed to determine the emission rate of any low energy (<30 keV) photon-emitting source. The gaseous proportional counter has the property that the detection efficiency can be varied by changing the pressure of the counting gas. For a multiwire proportional counter (MWPC), a maximum occurs in the variation of gas efficiency with pressure. It is shown below that, if the counting rates of photons from any two sources are maximized by varying the pressure, the detection efficiency of the center counter is the same for both sources and its absolute value is only dependent on the ratio of two geometrical distances which define the center and ring counters.

In the following proof, assume that a narrow parallel beam of photons is incident normal to the counter window and

the operation of the center counter in anticoincidence with the ring counter eliminates all contributions due to the wall effect. The distances a and b are shown in Fig. 8. The counting rate of the center counter is given by the following expression:

$$C_{CC} = I_0 e^{-(\mu/\rho)\rho a} - I_0 e^{-(\mu/\rho)\rho(a+b)} \quad (4)$$

where C_{CC} is the counting rate of the center counter; I_0 is the number of photons/sec of the beam entering the proportional counter; (μ/ρ) is the mass attenuation coefficient in cm^2/g ; and ρ is the density of the counting gas (in g/cm^3) which is proportional to the gas pressure.

The efficiency of the center counter can be obtained by dividing both sides by I_0 :

$$\epsilon_{CC} = \frac{C_{CC}}{I_0} = e^{-(\mu/\rho)\rho a} - e^{-(\mu/\rho)\rho(a+b)} \quad (5)$$

This equation is valid in the absence of wall effect, which is assumed to be eliminated completely by the anticoincident ring counter. One can maximize the efficiency and solve for ρ_{max} :

$$\frac{\partial \epsilon}{\partial \rho} = 0 = -a \left(\frac{\partial (\mu/\rho)}{\partial \rho} \rho_{\max} + \mu/\rho \right) e^{-(\mu/\rho) \rho_{\max} a} +$$

$$(a+b) \left(\frac{\partial (\mu/\rho)}{\partial \rho} \rho_{\max} + \mu/\rho \right) e^{-(\mu/\rho) \rho_{\max} (a+b)} \quad (6)$$

$$a e^{-(\mu/\rho) \rho_{\max} a} = (a+b) e^{-(\mu/\rho) \rho_{\max} (a+b)} \quad (7)$$

$$\frac{a}{a+b} = e^{-(\mu/\rho) \rho_{\max} b} \quad (8)$$

$$\ln \left(\frac{a}{a+b} \right) = -(\mu/\rho) \rho_{\max} b \quad (9)$$

$$\ln(1+b/a) = (\mu/\rho) \rho_{\max} b \quad (10)$$

Thus,

$$\rho_{\max} = \frac{\ln(1+b/a)}{(\mu/\rho) b} \quad (11)$$

ρ_{\max} can then be substituted into equation 5 to obtain ϵ_{\max} :

$$\epsilon_{\max} = e^{-\frac{a[\ln(1+b/a)]}{b}} - e^{-\frac{(a+b)[\ln(1+b/a)]}{b}}$$

Therefore,

$$\epsilon_{\max} = (1+b/a)^{-a/b} - (1+b/a)^{-(1+a/b)} \quad (12)$$

The validity of the several assumptions in this proof will now be discussed. First, the shape of the beam entering the counter is in reality a cone and not a parallel beam. However, this cone can be thought of as an infinite number of infinitesimally small diameter parallel beams, each with slightly different values of \underline{a} and \underline{b} . Thus one can find an "effective" beam which represents an average of all beams comprising the cone. Equation 12 remains valid for the "effective" beam provided that \underline{a} and \underline{b} are replaced by weighted mean values. The essential point that ϵ_{\max} is energy independent is preserved, although the value of ϵ_{\max} will be slightly different for the cone than for the parallel beam assumed above. To determine the magnitude of this effect, two calculations were performed. The values of ρ_{\max} and ϵ_{\max} were determined for a beam along the central line of the cone and for a beam on the surface of the cone. This cone is defined by the diameter of the window and the distance from the source to the window. The "effective" beam would have values of \underline{a} and \underline{b} between those of the two beams under consideration. The results of these calculations are shown in Table 4. It can be seen that the pressure necessary for maximum count-rate is essentially unchanged by the effect of the cone. However, the absolute value for the maximum efficiency is altered, and therefore, the efficiency must be determined experimentally.

Table 4. Effects of the Conical Photon Beam

Line	<u>a</u> (cm)	<u>b</u> (cm)	ρ_{MAX} (g/cm ³)	ϵ_{MAX}
Center of the Cone	4.76	5.08	0.002278	0.262
Surface of the Cone	4.87	4.82	0.002279	0.249

The second assumption is that the values of a and b do not change with pressure. In order to show this to be true, a computer program, which is given in Appendix A, was written to plot the efficiency vs pressure curve defined by equation 5 and at the same time plot the experimental count-rates. Both the theoretical and experimental curves were normalized to the maximum, in order to compare the shapes of these curves. The count-rates as a function of pressure were obtained for the K x rays of arsenic (10.5 keV) and the 14.4 keV γ -rays of Co^{57} . The results of the computer programs for the two sources are given in Fig. 6. As the same values of a and b were used in both cases, and the shape of the curves is in agreement, it is concluded that the change in pressure does not effect the size of the center counter, and hence, of a and b.

The last assumption to be discussed is that the size of the center counter does not vary with voltage. Karttunen has reported¹⁰ that the center counter varies in effective diameter as bias is applied to the counting wires of the ring counter. A series of runs were made varying the cathode voltage from -2800 volts to -4700 volts. It was necessary to carry out runs at different pressures, as the electronic system would only allow a spread of about 700 volts at one pressure. However, there were overlapping points to assure some consistency. The results are shown in Fig. 7. Since the count-rates are constant over this region, it was

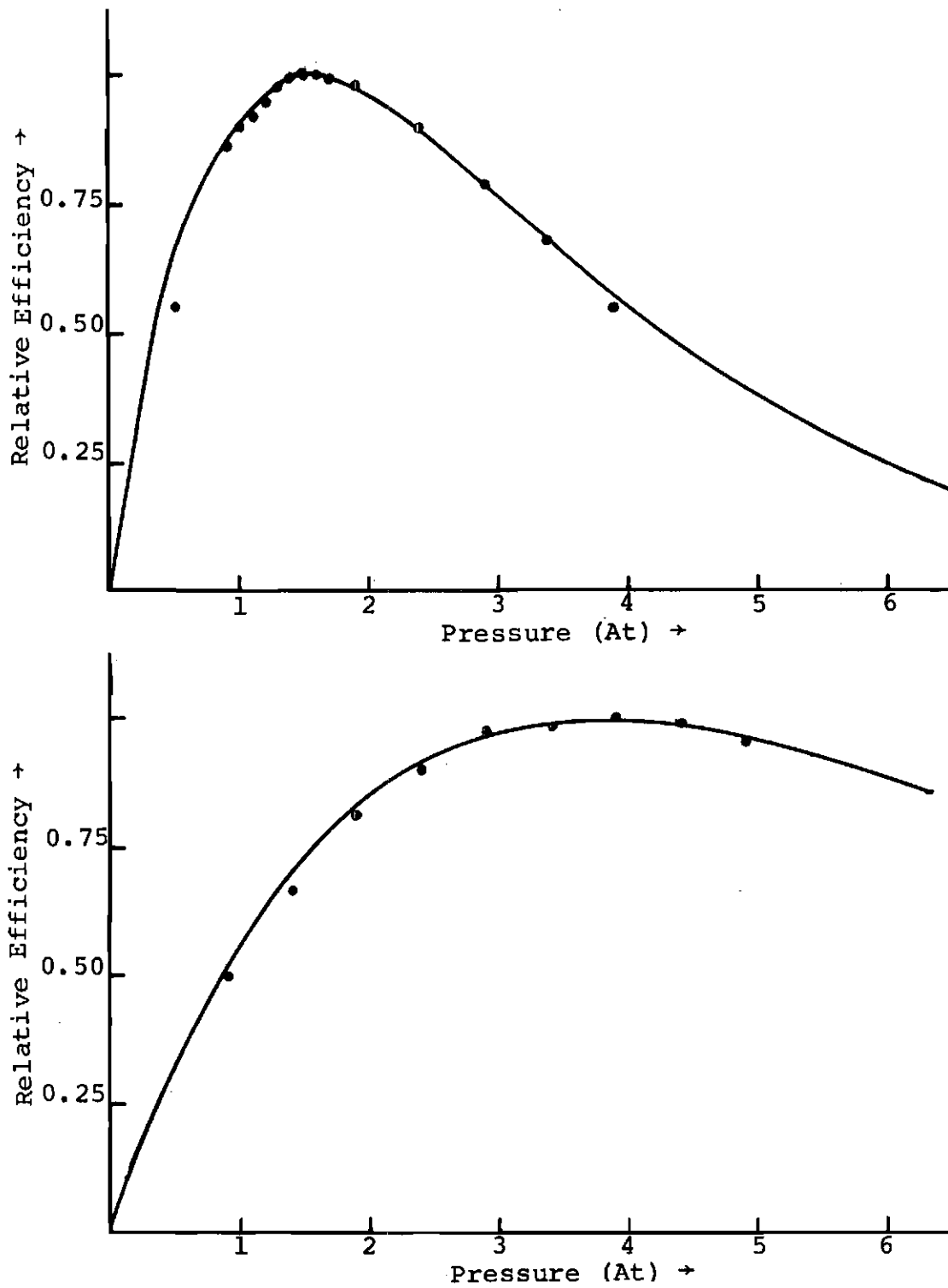


Fig. 6. Comparison of Experimental and Calculated Efficiency-Pressure Curves.

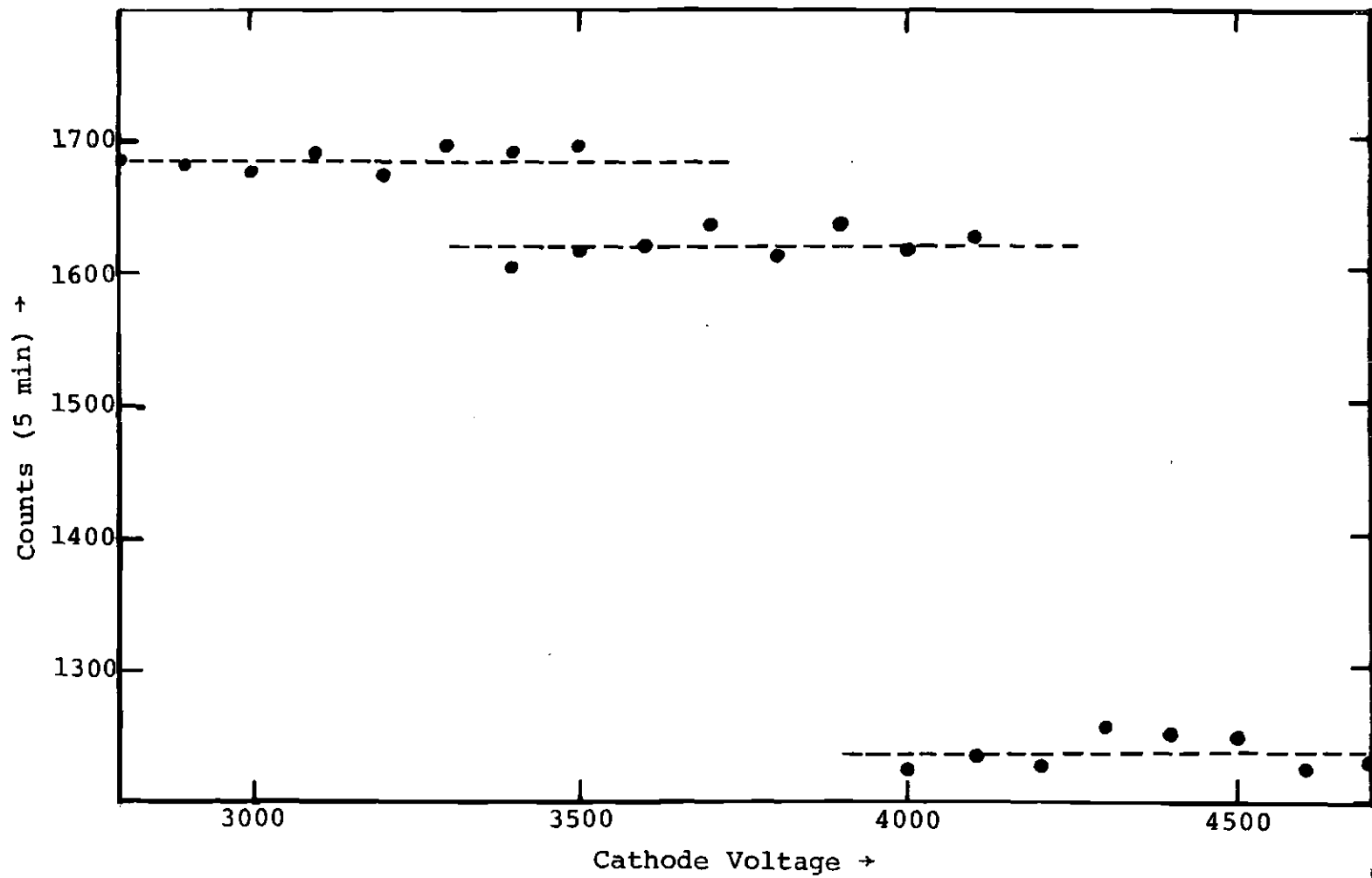


Fig. 7. Count-Rate - Voltage Curves.

concluded that the center counter does not change size with a change of voltage. This does not disagree with the work of Karttunen¹⁰. In a multiwire proportional counter with center counter walls defined by a set of cathode wires, the sensitive counting volume is affected by the electric fields present in the ring and center counters and will therefore generally not be identical with the nominal geometric volume. In order to change the center counter volume to agree with the geometric volume to permit use of μ/ρ tables in determining the efficiency of the center counter, Karttunen applied a negative potential on the anode wires of his ring counter, which led to three different potentials in the counter: (1) a negative voltage or bias on the counter wall and cathode wires, (2) a smaller negative bias on the anode wires of the ring counter, and (3) a floating potential on the center counter counting wire. In the present work, a knowledge of the actual sensitive volume of the center counter is not needed, as the method is independent of the mass attenuation coefficient, and the only requirement on this volume is that it remain constant with a change of bias placed on the walls and cathode wires of the counter. Also, in the much smaller multiwire proportional counter used by Karttunen, the ratio of a/b , defined geometrically by counter dimensions, is very much smaller than that of the counter in the present work and is therefore more susceptible to alteration of center counter sensitive volume by a change of the electric fields. However both Karttunen's

method and the present method of absolute efficiency determination depend on the use of calibrated radioactive standards.

It was found that the size of the present center counter is smaller than that determined by the position of the cathode wires. The $\epsilon\Omega$ product for the proportional counter was measured by two different standard sources (Y^{88} and Co^{57}) for both an uncollimated and a collimated geometry. The ratios of uncollimated to collimated $\epsilon\Omega$ products for both sources agreed with the calculated ratio of solid angles. The proportional counter detection efficiency ϵ was considerably smaller than that obtained from a calculation from equation 12, and the discrepancy was larger than one would expect from the effect of the conical beam rather than the parallel beam as discussed above. Therefore, the center counter sensitive volume must indeed be smaller than geometrical, as determined by the cathode wires. The actual size of the center counter has not been determined, as the only quantity necessary is the product $\epsilon\Omega$.

3.2.2. Apparatus and Electronic System. The multiwire proportional counter used in this experiment has been described previously¹¹. It is 15 liters in volume and has a geometrical center counter diameter of 5.08 cm and a total diameter of 14.6 cm. A source holder of plexiglass was built such that the source was 10.22 cm from a 0.56 cm thick beryllium window. The cone of photons entering the proportional counter is defined by the inside opening in the wall which is 0.95 cm in diameter and 1.05 cm from the

beryllium window. A collimator of 0.58 cm diameter, made of brass (the same material as the counter wall), could be fitted inside the source holder. The source holder arrangement is shown in Fig. 8.

A block diagram describing the electronics is shown in Fig. 9. The ring counter pulses are fed through a preamplifier and amplifier to a discriminator set just below the energy of the K x rays of argon (2.82 keV). The resulting logic signals are used to gate the first stage of a dual linear gate(LG-1).

The main path of the linear center counter pulses is shown by the heavy line in Fig. 9. The signals are fed through a preamplifier, amplifier, and delay amplifier(DA-1) to the input of the first stage of the dual linear gate(LG-1). This unit is set to pass only those pulses not coincident with the ring counter. The variable gate width was set at 15 μ sec, in order to completely encompass the 10 μ sec wide bipolar linear pulse. The output signals of LG-1 were then delayed and fed into the input of the second stage of the dual linear gate(LG-2). This gate is used only when setting the single-channel analyzers and will be described below. The signals from this gate are then fed into two 128-channel multichannel analyzers. The first, MCA-1, holds the center counter spectrum, while the second, MCA-2, is used in the external multiscaler mode which uses pulser P to set the duration of time for each channel.

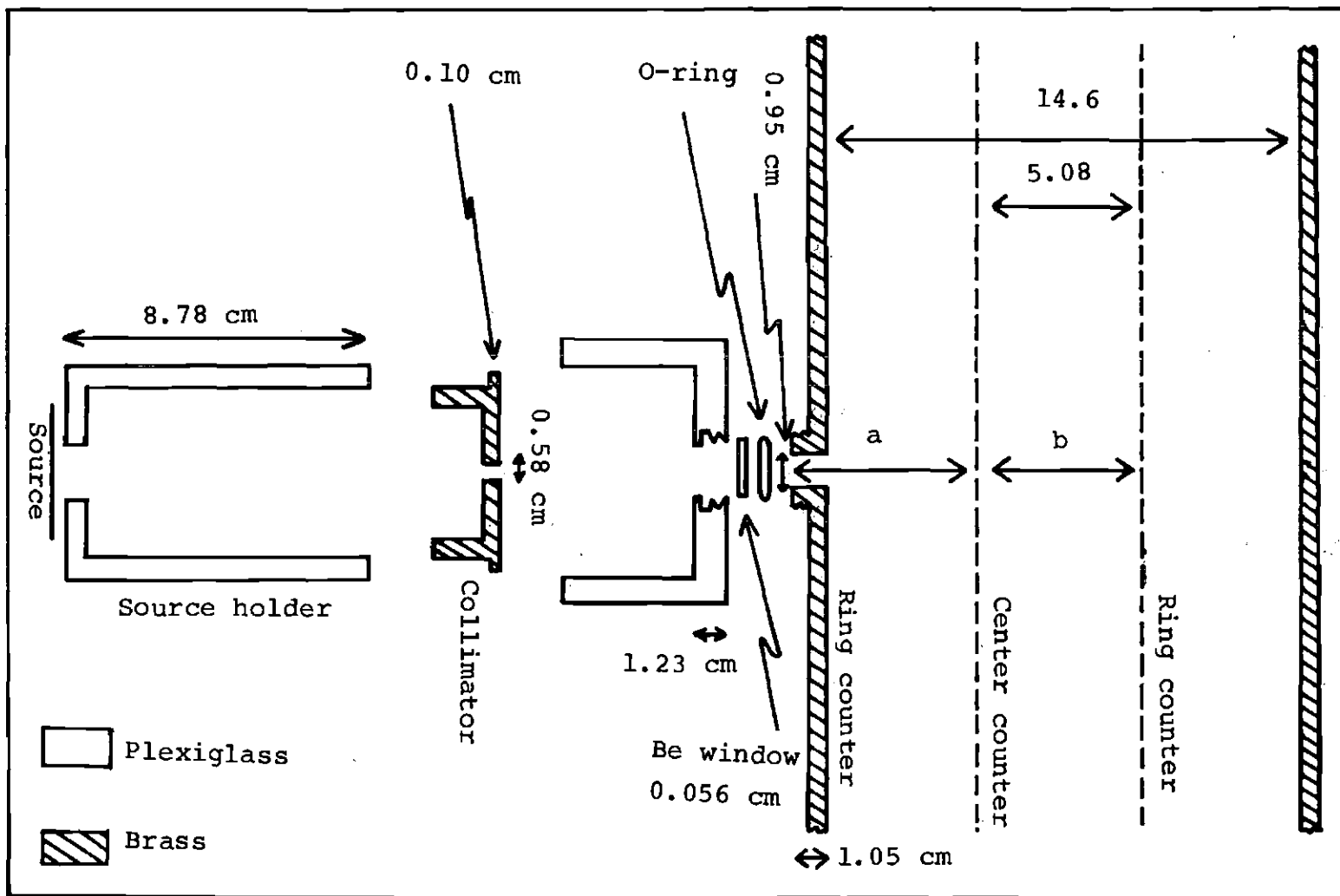


Fig. 8. Source holder arrangement for the Proportional Counter.

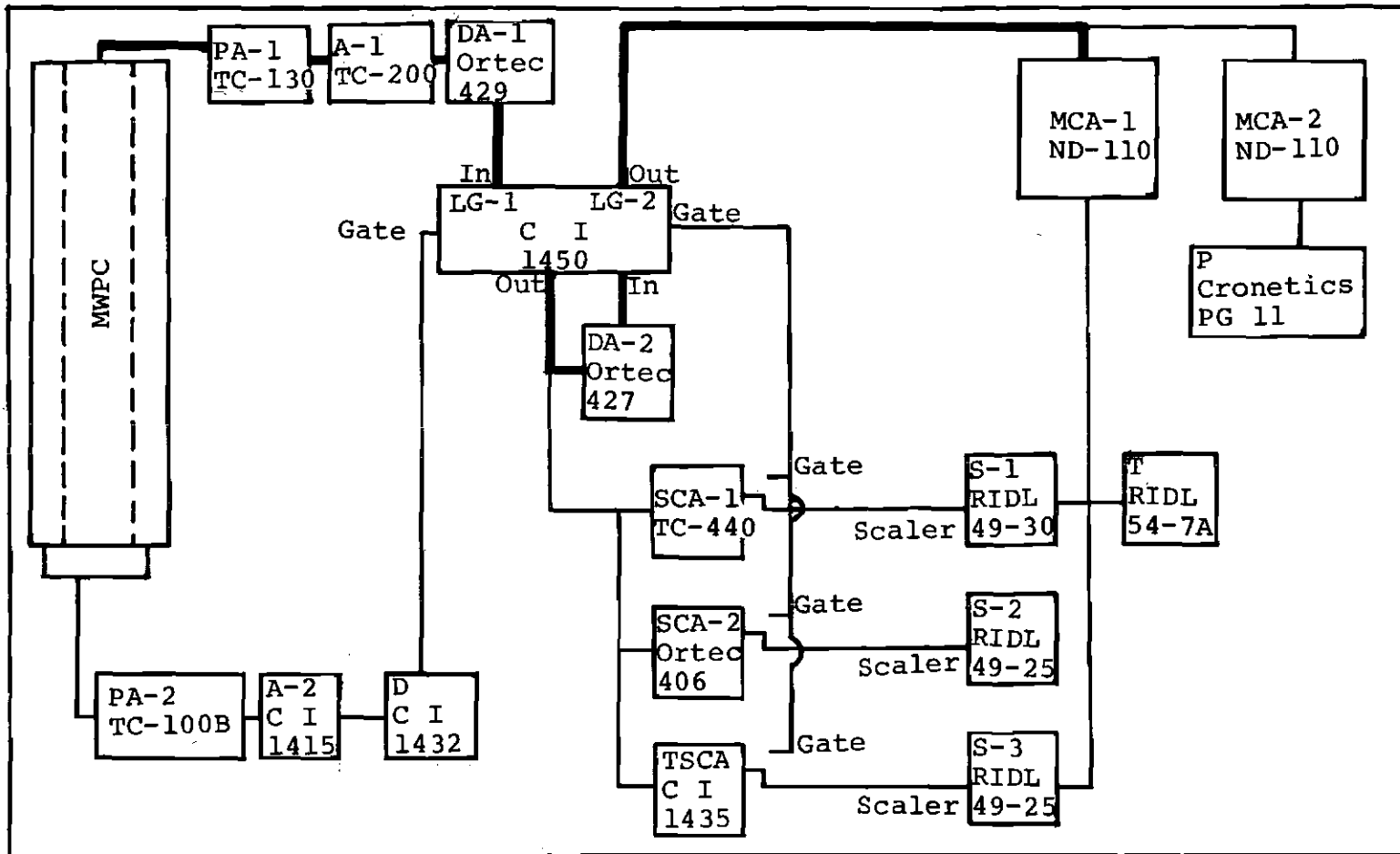


Fig. 9. Block Diagram for the Standardization of Sources. The following abbreviations are used: MWPC - multiwire proportional counter; A - linear amplifier; PA - preamplifier; DA - delay amplifier; D - discriminator; SCA - single channel analyzer; MCA - multichannel analyzer; LG - linear gate; TSCA - timing single channel analyzer; S - scaler; T - timer; P - pulse generator.

This system was used to check for variations in counting rate during a run.

The output of LG-1 is also fed into three single-channel analyzers (SCA-1, SCA-2, and TSCA). These single-channel analyzers are set respectively on a region below, on, and above the peak of interest by means of self-gated spectra which were taken with the output of the individual single-channel analyzers connected to the gate input of LG-2.

3.2.3. Procedure. Several experimental difficulties were encountered in the application of the method presented in Sect. 3.2.1. The pressures necessary to obtain the maximum counting rate of the desired photons allowed a very large transmission of the high energy γ -rays present in the Se^{75} , Co^{57} , and Y^{88} sources which were used in this investigation. When these γ -rays impinge on the counter wall, secondary radiations are produced, for example photoelectrons and Compton-scattered photons. Operation of the multiwire proportional in the anticoincidence mode not only greatly reduced the natural background, but also eliminated the effects of photoelectrons which originate in the counter wall. However, Compton photons may pass through the ring counter without triggering the anticoincidence gate, and a subsequent Compton scattering in the center counter may produce a pulse in the energy region of interest. A background run obtained by placing an absorber between

the source and the counter, in order to remove only the low-energy photon of interest was necessary to measure the magnitude of this effect.

A previous investigation left radioactive Fe^{55} in the form of ferrocene adsorbed on the wall and wires of the counter. An attempt to remove the Fe^{55} by cleaning the counter with organic solvents reduced, but did not eliminate, this problem. After the counter was evacuated and filled to the proper pressure, a peak due to the decay of the iron slowly "grew" into the spectrum. The nuclide Fe^{55} decays by pure electron capture to the ground state, and therefore exhibits only a 5.9 keV line due to the resulting manganese K x rays and Auger electrons. Although this was completely resolved from the 10.5 keV arsenic K x rays, it did affect the "tail" region of the spectrum below the peak of interest. It was therefore necessary to keep the contribution due to the Fe^{55} essentially the same during both the main and background runs. This could only be accomplished by taking a spectrum for less than 2 hours followed immediately by a background run.

Radiofrequency noise due to a gas chromatograph located in the Chemistry Building was also found to be a problem. Careful shielding and grounding of the equipment reduced the noise considerably. However, there were noise signals, which went through all gates and single-channel analyzers, that appeared at irregular intervals and had

pulse heights in the energy region of 2-20 keV. The three scalers and the multichannel analyzer MCA-2 were used as a check, in order to reject runs in which spurious pulses occurred.

Runs were taken for two different Co⁵⁷ sources (labeled A and B), an Y⁸⁸ IAEA standard source, and the Se⁷⁵ source. Since many runs were taken for all the sources, a computer program was written which stripped background, plotted spectra from the run, the background, or background-subtracted spectrum, and summed any region of all three. This program is presented in Appendix B.

3.3 Evaluation of ϵ_K

The proportional counter data, which lead to the detection efficiency of the Si(Li) detector ϵ_K is presented in Table 5. This efficiency was determined by the following expressions:

$$\epsilon_K = \frac{C_K \{ \text{Si(Li)} \}}{N_0 (\text{Se}^{75})} \quad (13)$$

where ϵ_K is the detection efficiency of the Si(Li) detector; $C_K \{ \text{Si(Li)} \}$ is the counting rate of the As K x rays in the Si(Li) detector; and

$$N_0 (\text{Se}^{75}) = \frac{C_K (\text{MWPC})}{\epsilon \Omega} \quad (14)$$

Table 5. Data Used to Determine ϵ_K

Source	Photon	Energy keV	Pressure of Ar (At)	Corrected [†] Count Rate c/sec	Emission Rate c/sec	ϵ_Ω	N_0 Se^{75} from ϵ_Ω c/sec	ϵ_K^*
Y^{88}	X Ray	14.4	3.8	18.02	2.25×10^5	8.00×10^{-5}	2.43×10^4	5.00×10^{-3}
Co^{57} A	γ -Ray	14.4	3.8	1.19	1.49×10^4	8.01×10^{-5}	2.45×10^4	4.95×10^{-3}
Co^{57} B	γ -Ray	14.4	3.8	8.97	1.13×10^5	7.92×10^{-5}		
Se^{75}	X Ray	10.5	1.6	1.94	—	—	—	—

[†] corrected for beryllium window, air, and (if necessary) polyethylene.

* using 16.78 c/sec as the Si(Li) detector counting rate of the Se^{75} source.

where C_K (MWPC) is the counting rate of the As K x rays in the multiwire proportional counter; and:

$$\epsilon\Omega = \frac{C_S \text{ (MWPC)}}{N_0 \text{ (S)}}$$

where $\epsilon\Omega$ is the efficiency-solid angle product; C_S (MWPC) is the counting rate of the standard S; and N_0 (S) is the absolute emission rate of the photon of interest from the standard S. All counting rates used were corrected for absorption and for half life. This procedure was used to obtain a value for ϵ_K through the use of both the Y^{88} IAEA standard and the two Co^{57} sources. The emission rates of the 14.4 keV γ -rays from the two Co^{57} sources were obtained by comparison with an IAEA Co^{57} standard on a Ge(Li) detector. The two $\epsilon\Omega$ products obtained from the two Co^{57} sources agreed within a 1σ statistical error and were combined with a weighting factor inversely proportional to σ^2 .

The value of ϵ_K determined through the Y^{88} standard was adopted, since the uncertainty in the K x rays/disintegration in this case was much smaller than that in the 14.4 keV γ -rays/disintegration for Co^{57} . Also there was no apparent "tail" in the spectra of Se^{75} and Y^{88} , and there was a larger background below the peak than above it in the spectra of Co^{57} . Therefore, there were two additional sources of error associated with the value of ϵ_K

obtained through the use of the Co^{57} sources that were not present in the value obtained through the Y^{88} IAEA standard. The final value of the detection efficiency for the Si(Li) detector is:

$$\epsilon_K = (5.00 \pm 0.19) \times 10^{-3}.$$

The efficiency curve at the 5 cm geometry is again presented in Fig. 10, with the As K x-ray point included. One possible reason for the increase in efficiency from 14.4 keV to 6.4 keV is that there is more incomplete charge collection (tailing) as the energy of the photons is increased.

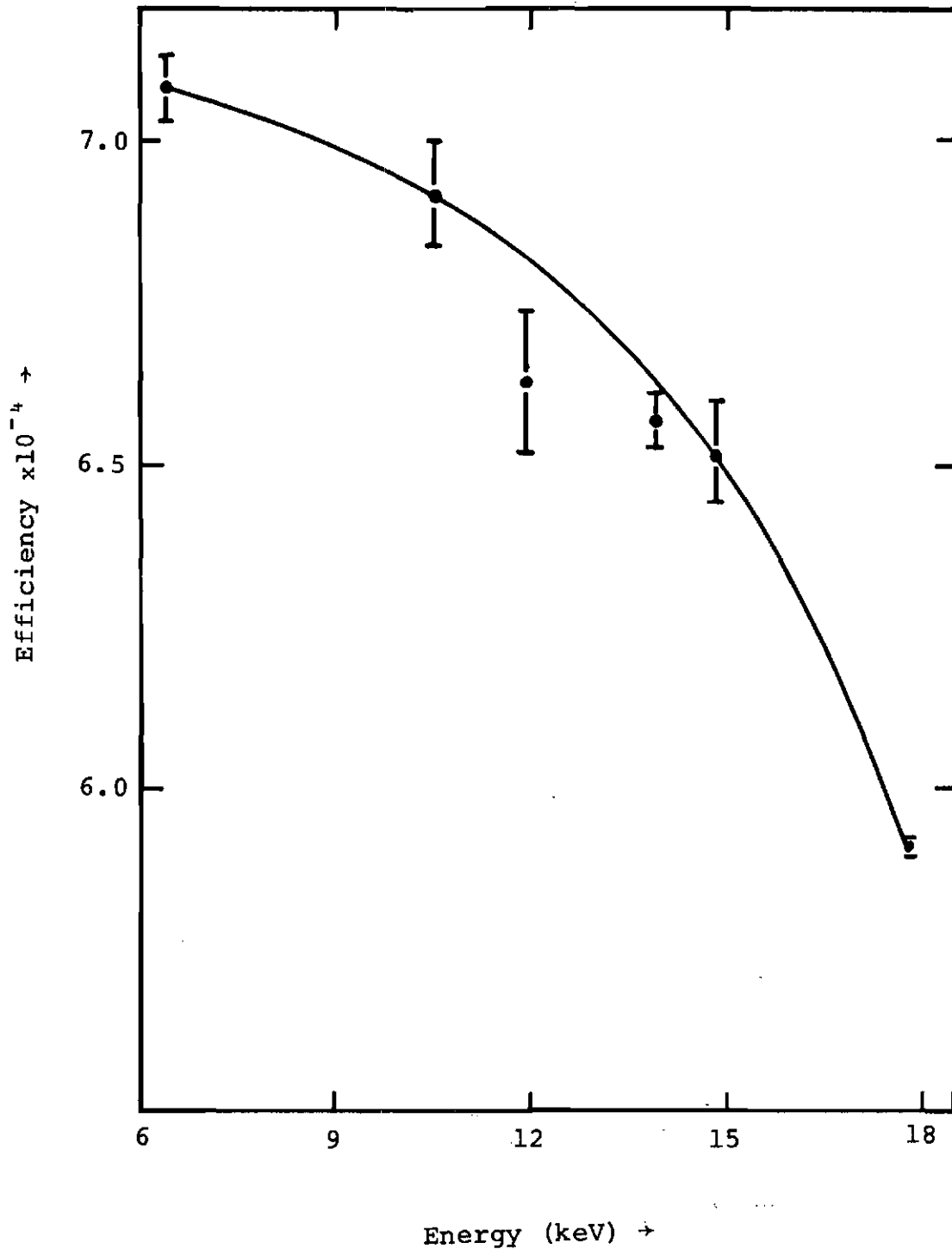


Fig. 10. Efficiency Curve of the Si(Li) Detector with the Se⁷⁵ Point Included.

CHAPTER IV

THE EVALUATION OF ω_K 4.1 Calculation of the Quantity P

In the absence of β^+ emission, the probability for K electron capture to a daughter state with energy E_γ above the ground state is given by:

$$P_K = \left[1 + \frac{P_L}{P_K} \left[1 + \frac{P_M}{P_L} \left(1 + \frac{P_N + P_O + \dots}{P_M} \right) \right] \right] \quad (16)$$

where P_X is the probability of electron capture to the X shell, where X is K, L, M, ... shell respectively.

From theory of electron capture^{1,2}, it can be shown that:

$$\frac{P_L}{P_K} = \frac{q_{L1}^2 \left(\frac{|\Psi_{L1}(0)|^2}{|\Psi_K(0)|^2} \right) \left(\chi^{L/K} + \frac{q_{L2}^2 \cdot \frac{|\Psi_{L2}(0)|^2}{|\Psi_{L1}(0)|^2} \cdot \chi^{L2/L1}}{q_{L1}^2} \right)}{\quad} \quad (17)$$

where: q_X is $Q_{EC} - E_\gamma - B$ (binding energy of the x-shell electron of the daughter); $\Psi_X(0)$ is the value of the wave function of the X-shell evaluated at the nucleus; and $\chi^{X1/X2}$ is the Bahcall exchange correction between the X_1 and X_2 shells. Also:

$$\frac{P_M}{P_L} = \frac{q_{M_1}^2 \left(\frac{|\Psi_{M_1}(0)|^2}{|\Psi_{L_1}(0)|^2} \right)}{q_{L_1}^2 \left(\frac{|\Psi_{L_2}(0)|^2}{|\Psi_{L_1}(0)|^2} - \frac{|\Psi_{M_2}(0)|^2}{|\Psi_{M_1}(0)|^2} \right)} \left(\chi^{M/L} + \frac{|\Psi_{L_2}(0)|^2}{|\Psi_{L_1}(0)|^2} - \frac{|\Psi_{M_2}(0)|^2}{|\Psi_{M_1}(0)|^2} \right) \quad (18)$$

The quantity $\frac{P_N + P_O + \dots}{P_M}$, which has a very small effect

on P_K , can be extrapolated from Ref. 13.

Exact wave functions for the different atomic states are not available, but several authors have derived approximate wave functions and exchange correction factors. A listing of quantities necessary in the calculation of P_K in Se^{75} decay is given in Table 6. These quantities and energy values (Q_{EC} , E_γ , and B) from Lederer, Hollander, and Perlman¹⁴, were used to calculate P_K for the electron capture of Se^{75} to the 400.7 keV level in As^{75} . The average of all the various permutations is: $P_K = 0.875 \pm 0.008$. The error limit given is twice the difference between the largest value and the smallest value obtained in these calculations. As demonstrated by the calculations above, it has recently been found¹⁵ that the theoretical P_L/P_K ratios do not significantly vary among the different wave functions and exchange corrections that are available, and, therefore, a better criteria for comparing the different theories is the P_M/P_L ratio. With this ratio it was shown¹⁵ that the best fit of allowed orbital electron capture theory to experiment in the region $18 \leq Z \leq 36$ is that based on the

Table 6. Theoretical Quantities Used in
the Evaluation of P_K

Quantity	Value	Reference
$\frac{ \Psi_{L_1}(0) ^2}{ \Psi_K(0) ^2}$	0.1027*	20
	0.1033	21
	0.1035	22
	0.1037	23
$\frac{ \Psi_{L_2}(0) ^2}{ \Psi_{L_1}(0) ^2}$	0.0103*	21
	0.0102	22
	0.0103	23
$\frac{ \Psi_{M_1}(0) ^2}{ \Psi_{L_1}(0) ^2}$	0.156*	24
	0.171	21
$\frac{ \Psi_{M_2}(0) ^2}{ \Psi_{M_1}(0) ^2}$	0.0107*	21
$\frac{P_N + P_O}{P_M}$	0.12(est.)*	13

Table 6. (Cont.)

Quantity	Value	Reference
$\chi^{L/K}$	1.096	25
	1.097	26
	1.091*	27
χ^{L_2/L_1}	0.914*	22
$\chi^{M/L}$	1.141	25
	1.088	22
	1.148	26
	1.088*	27

Watson-Freeman wave functions²⁴ and the Vatai²⁷ electron exchange-overlap correction. Using this combination (i.e. those quantities starred in table 6), the theoretical value of P_K in Se^{75} decay to the 400.7 keV level in As^{75} is:

$$P_K = 0.876 \pm 0.004.$$

The error limits are due to a 5 percent uncertainty in the ratio of P_L/P_K , which was determined from the comparison of experiment to theory by Genz¹⁵. The uncertainties in the other quantities used in the calculation give a negligible contribution to the error limits.

4.2 Final Result and Evaluation of Errors

The final result for the K shell fluorescence yield for arsenic is:

$$\omega_K = 0.589 \pm 0.027.$$

The error limit is the 2σ statistical error added linearly to the systematic error. The value is obtained from the measurements of the $P_K \omega_K \epsilon_K$ product (Chapter II), with P_K evaluated from theory (Sect. 4.1), and ϵ_K evaluated as discussed in Sect. 3.3.

An especially careful evaluation of the above error limit was performed in the following way. Results of the measurements and the calculations used in the evaluation

are presented in Table 7, along with the individual errors. The proportional counter counting rate for the Y^{88} IAEA standard includes a 0.9 percent uncertainty coming from both the total statistical 1σ error from the sum of the runs and the spread of the individual runs. This was handled on the assumption that the error is purely statistical. The emission rate of the K x rays of strontium from the Y^{88} IAEA standard contains a 1.0 percent systematic error arising from the uncertainty in its $P_K \omega_K$ product and from the IAEA standardization. The proportional counter counting rate of As K x rays from the Se^{75} source has associated with it a 1.0 percent error of the same nature as the counting rate from the Y^{88} standard. The counting rate of the As K x rays in the Si(Li) detector has a 0.5 percent 1σ statistical error. In order to obtain the detection efficiency in the coincidence geometry, a ratio of counting rates at the coincidence geometry compared to the more reproducible 5 cm geometry must be obtained, and this ratio has associated with it a 0.85 1σ statistical error. The errors in the $P_K \omega_K \epsilon_K$ measurement and the P_K calculation have been discussed in Sects. 3.3 and 4.1 above. The statistical errors have been quadratically combined, doubled to obtain a 2σ error (95.5 percent confidence level), and added linearly to the systematic errors. The errors in the method used to calibrate the Se^{75} K x-ray emission rate on the proportional counter are believed to

Table 7. The Errors in the Evaluation of ω_K

Item	Value	Errors [†]	
		Statistical*	Systematic
Y^{88} Count-Rate (MWPC)	17.93	0.9	-
Y^{88} Emission-Rate	2.253×10^5	-	1.0
Se^{75} Count-Rate (MWPC)	1.941	1.0	-
Se^{75} Count-Rate (Si (Li))	16.78	0.5	-
Close/Far Geometry	7.22	0.85	-
$P_K \omega_K \epsilon_K$	0.00158	0.5	-
P_K	0.876	-	0.4
Total	-	1.67	1.4
Final			4.60

[†] in percentage.

*a 1σ error.

be negligible compared to the statistical errors. The value of ω_K at $Z=33$ obtained through the use of Co^{57} calibration sources is 0.595 ± 0.038 . The good agreement of the two values obtained through the use of the Y^{88} and Co^{57} standard sources indicates that the error in the method is small in comparison to the total error. As stated previously, the value of ω_K obtained through the use of the Y^{88} standard is adopted only because it has a smaller error associated with it than does the corresponding value from the Co^{57} sources.

CHAPTER V

DISCUSSION

5.1 Comparison with Theory

Three different theoretical curves of ω_K , in the region of $Z=26$ to $Z=43$, are shown plotted against Z in Fig. 11. The values of ω_K for $Z=33$ obtained from these theories are presented in Table 8. The best agreement for the present value and for the "most reliable" values¹ based on gaseous techniques, is with the theory of McGuire¹⁶. However, only four values from McGuire's theory exist in the region $25 \leq Z \leq 43$, so that significant errors might arise from interpolation. The theoretical results of Kostroun, Chen, and Crasemann¹⁷ and Walters and Bhalla¹⁸ agree reasonably well with these experimental points. However, as has been pointed out previously¹, the theory of Walters and Bhalla¹⁸ does not include all of the Auger transitions and therefore slightly overestimates the values of the K shell fluorescence yields.

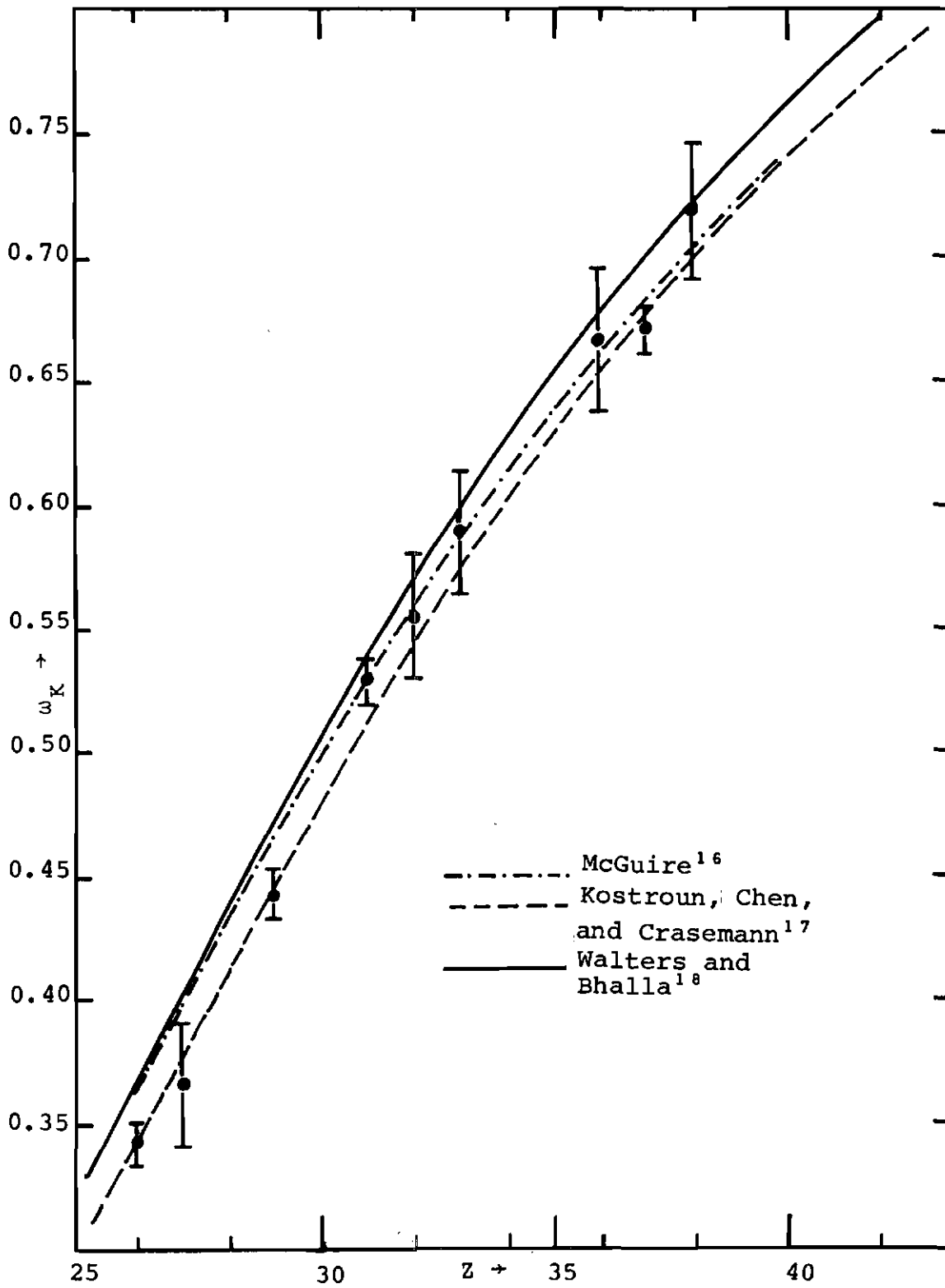


Fig. 11. Theoretical Curves of ω_K , $25 \leq Z \leq 43$.

Table 8. Theoretical Values for ω_K at $Z=33$

Author	ω_K
McGuire ¹⁶	0.584 (from curve)
Kostroun, Chen, and Crasemann ¹⁷	0.574
Walters and Bhalla ¹⁸	0.595
"Best Fit" ¹	0.567±0.031
Present Experimental Value	0.589±0.027

5.2 Comparison of the Gaseous and Solid Methods in

Determining ω_K in the Region $25 < Z < 43$

Pahor, Kodre, and Moljk⁹ have determined the K shell fluorescence yield of arsenic to be $\omega_K = 0.587 \pm 0.003$, where the error limits are the 1σ statistical error. This work employed the method of external fluorescent excitation of gaseous AsH_3 in a multiwire proportional counter. This result is in excellent agreement with the value 0.589 presented in this thesis and demonstrates that there should be no intrinsic difference in the results from the gaseous and solid source methods, if these experiments are properly performed.

In the method of Pahor, Kodre, and Moljk⁹, the spectrum consists of a "full energy" peak and an "escape" peak. If the counter is at sufficiently low pressure, the K x rays from the target gas almost completely escape the counter. The Auger electrons do not escape, but instead sum with the photoelectrons to yield pulses in the peak corresponding to the full energy of the incident photon. Those events where a K x ray of the target gas escapes the center counter are seen as a peak at an energy decreased by the energy of the escaping K x ray of the target gas. The main source of error in this method arises from the correction necessary due to those photoelectric events which occur in higher electron shells. These events lead to

pulses in the "full energy" peak, and in order to correct for this, a value of the "K-jump" is needed. The "K-jump" is the ratio of the photoelectric absorption coefficient for all the electron shells to the same coefficient for the K shell only. The lack of a precise value of the "K-jump" adds at least 5 percent to the measurement at $Z=33$. The other errors in this method are similar to those of the internal gaseous radioactive source method (to be discussed next), and a more precise knowledge of the "K-jump" would make this method comparable in accuracy.

Of all the methods used in the determination of ω_K in the low-to-middle- Z region, the most accurate is that using an internal gaseous radioactive source in a multiwire proportional counter. Freund et al.^{11-a} and Pahor, Kodre, and Moljk¹⁹ both used this method to determine ω_K of gallium by using a radioactive gaseous Ge^{71}H_3 source. In this method, a high- Z counting gas at high pressure was used to obtain the total K x-ray and K-Auger electron counting rates. A second run using a low- Z counting gas at low pressure was used to obtain the K-Auger electron counting rate, since the K x rays almost completely escape the center counter. A small correction is needed to account for the x rays which are seen in the center counter during the low pressure run. The magnitude of this effect can be determined from a triple integral as was demonstrated in ref. 11-a. There is also

a small correction necessary due to the degradation of the Auger or photoelectrons, if they pass through the weak field regions between the ring and center counters. The magnitude of this effect can be obtained experimentally by taking singles runs in both the center and ring counters, adding the two and comparing this to the summed spectra of the ring and center counter. A good description of the manipulations of these data is given in ref. 11-a. With a careful analysis of these effects, the total error of this method can be reduced to less than one percent. There are serious limitations to the applicability of the gaseous techniques as many of the ideal sources or targets cannot readily be converted to a suitable gaseous form.

The largest source of error in the $P_K \omega_K \epsilon_K$ method used in this work is in the efficiency ϵ_K . This error is due primarily to the necessity of calibrating the Se^{75} source (see Sect. 3.1). The errors associated with the efficiency contain the problem of self absorption, which can be minimized by using very thin solids-free radioactive sources, the uncertainties in the correction for the solid angle and absorption in air and in the beryllium window. The errors associated with the absorption corrections are normally negligible. The P_K calculation adds a linear systematic error, but, as discussed in Sect. 4.1, the error in this is small in comparison with the errors in the efficiency. The errors in the coincidence measurement

are essentially statistical in nature and can therefore be minimized. However, the total error in this method cannot be reduced much below 2 percent, owing to uncertainty in the efficiency ϵ_K .

5.3 Suggestions for Further Research

In the region $39 < Z < 46$ there are no "reliable" experimental values of ω_K^1 . The $P_K \omega_K \epsilon_K$ method could be applied to four other possible cases in this region of Z.

The decay of 85-day Zr^{88} proceeds by 100 percent electron capture to the 394 keV level in 108-day Y^{88} . The resulting γ -ray is only weakly converted and there is no other feeding of the 394 keV level. This would be an ideal case if the 394 keV level were not an isomeric transition with a 0.3 millisecond half-life. It would therefore be necessary to use a large resolving time (about 1 millisecond) in order to avoid large corrections in the coincidence efficiency. This in turn would require a weak source to keep the chance coincidences acceptably small.

The decay of 10.16-day Nb^{92m} proceeds through electron capture to the 1.83 MeV (2.7%) and 934 keV (97.2%) levels of Zr^{92} . The 1.83 MeV level decays 68 percent to the 934 keV level, and a correction of about 2 percent would have to be applied if the 934 keV γ -ray were used as the gating pulse. The 1.83 MeV γ -ray could also be used, but its low intensity and small detection efficiency would

make necessary a strong source resulting in a large correction for chance coincidences. The stronger 900 keV γ -ray from the decay of the 1.83 MeV level to the 934 keV level, could be used, although a correction would be necessary for the small internal conversion of the 934 keV transition.

A similar situation exists in the case of 4.5-day $\text{Rh}^{101\text{m}}$. It decays by electron capture to both the 544.5 keV(6%) and the 306.7 keV(84%) levels. It may be possible to use the 306.7 keV gamma transition to the ground state as the gating signal. Also the 544.5 keV γ -ray and the 237.8 keV γ -ray resulting from the decay of the 544.5 keV to the 306.7 keV levels, could be used with the same considerations as with the Nb^{92} case.

The fourth case is $\text{Ag}^{108\text{m}}$, which has a half-life larger than 5 years. It proceeds by 90 percent electron capture to the 1.77 MeV excited state of Pd^{108} (and a 10 percent isomeric transition to the ground state). The 1.77 MeV level, however, deexcites through a cascade of three E2 transitions of energies 722, 614, and 434 keV, respectively. If the 722 keV gamma ray were used as the gating pulse, corrections for the weak internal conversion of the other two E2 transitions would be necessary.

All of these cases have certain difficulties associated with them, and therefore the errors associated with the final result would be correspondingly larger.

On the other hand, the gaseous methods are probably not feasible in the region $39 < Z < 46$, as this is the second transition metal series and conversion of these elements into suitable gaseous form would be extremely difficult.

One of the most significant contributions of this thesis is the new method for calibration of low energy radioactive sources (< 30 keV). Additional work should be done in order to obtain agreement of the calculated detection efficiency (equation 12) with experimental results. In order to do this, effective values of the proportional counter distance parameters a and b , discussed in Sect. 3.2.1, must be found, such that the calculated efficiency vs pressure curve agrees both in shape and absolute magnitude with experimental results. Also a confirmatory experiment should be made at a different energy, such as 6.4 keV (K x rays from a Co^{57} standard). This measurement would also be a valuable check of the K x ray to 14.4 keV γ -ray ratio in Co^{57} . A further refinement can be made to include the effects arising from the conical shape of the incident photon beam in the proportional counter (Sect. 3.2.1). One approach that could be taken is to determine the efficiency of individual parallel beams (of various incident angles) and then obtain a weighted average of these efficiencies which would accurately correspond to the geometrical situation.

APPENDIX A

EFFICIENCY VS PRESSURE COMPUTER PROGRAM

This computer program is used to compare the shape of the experimental efficiency-pressure curve with the curve calculated by equation 5. It is written in Fortran V for a remote terminal and needs little explanation for those familiar with the language. The user supplies the linear attenuation coefficient (at one atmosphere) of the counting gas, the pressure at which the user wishes to start and stop the comparison, the incremental pressure desired, and the values of the distance parameters a and b for the multiwire proportional counter (Sect. 3.2.1). The program calculates the efficiency for those pressures determined by the values read into the computer, and then normalizes the results such that the maximum efficiency is unity. the user then feeds the number of experimental points and then the values of the points themselves, which have been previously normalized such that the maximum value is full scale. At this time the program plots the curve with the pressure at the left, the normalized value from equation 5 given with a *, the experimental point given as a #, and if the two values agree, a \$ is typed.

```

C EFFICIENCY VS PRESSURE
  DIMENSION E(999), CF(999), IPL(999), IARPY(60), AE(999), PX(50), IEX(50)
  WRITE(6, 1)
1  FORMAT(1X, ' WRITE MU(6.3), P ST, P SP, INC')
  READ(5, 2) XM, ST, SP, SINK
2  FORMAT(2X, F6.3, 2X, F5.2, 2X, F5.2, 2X, F5.2)
  WRITE(6, 8)
8  FORMAT(2X, ' WRITE A, B')
  READ(5, 9) A, B
9  FORMAT(2X, F5.2, 2X, F5.2)
  IQ=0
  IQQ=0
  JQ=0
  IZ=0
  IZZ=0
  IDELM=INT((SP-ST)/SINK)+1
  DO 100 I1=1, IDELM
  CF(I1)=ST+(SINK*(I1-1))
  F(I1)=EXP(-A*CF(I1)*XM)-EXP(-(A+B)*CF(I1)*XM)
  IQ=INT(E(I1)*100000.0)
  IF(IQQ-IQ) 50, 100, 100
50 IQQ=IQ
  JQ=I1
100 CONTINUE
  DO 130 I2=1, IDELM
130 AF(J1)=F(J1)/F(JQ)
  WRITE(6, 3)
3  FORMAT(4X, 2H P, 5X, 2H F, 5X, 3H AF)
  DO 150 I2=1, IDELM
  WRITE(6, 4) CF(I2), F(I2), AF(I2)
4  FORMAT(2X, F5.2, 2X, F5.4, 2X, F6.4)
150 CONTINUE
  WRITE(6, 10)
10  FORMAT(2X, ' WRITE NO. EXP. PNTS')
  READ(5, 11) I4
11  FORMAT(2X, I2)
  WRITE(6, 12)
12  FORMAT(2X, ' WRITE PRESSURE, NORM. EFF. ')
  DO 151 J2=1, IAA
  READ(5, 13) PX(J2), IEX(J2)
13  FORMAT(2X, F5.2, 2X, I2)
151 CONTINUE
  DO 200 I3=1, IDELM
  DO 199 I4=1, 60
  DO 153 J3=1, IAA
  IZ=INT((CF(I3)*100)-(PX(J3)*100))
  IF(IZ) 153, 152, 153
152 IZZ=1
  JZF=J3
153 CONTINUE

```

```
154 IPL(I3)=INT((F(I3)/E(J0))*60)
    IF(I77)165,165,155
155 CONTINUE
    IF(IPL(I3)-IEX(JRB))156,158,157
156 CONTINUE
    IF(IPL(I3)-I4)161,170,160
157 CONTINUE
    IF(IEX(JRB)-I4)159,180,160
158 CONTINUE
    IF(IEX(JRB)-I4)160,190,160
159 CONTINUE
    IF(IPL(I3)-I4)160,170,160
161 CONTINUE
    IF(IEX(JRB)-I4)160,180,160
165 CONTINUE
    IF(IPL(I3)-I4)160,170,160
160 IARPY(I4)= ' '
    GO TO 198
170 IARPY(I4)= '*'
    GO TO 198
180 IARPY(I4)= '#'
    GO TO 198
190 IARPY(I4)= '5'
198 JRB=0
    I77=0
199 CONTINUE
    WRITE(6,7)CF(I3),IARPY
    7 FORMAT(2X,F5.2,3X,60A1)
200 CONTINUE
    STOP
    END
```

APPENDIX B
SPECTRA STRIPPING COMPUTER PROGRAM

This program is also written in Fortran V for a remote terminal. This program is used to compare and strip two spectra. Two spectra, A and B, are fed into the computer (usually by paper tape) following which the computer types out the spectrum so that any necessary corrections can be made. At this point, the two spectra can be added, subtracted, or multiplied by any scaling factor. The resulting spectrum is labeled C, while A and B remain unchanged. Spectra A, B, and C can then be printed out (a paper tape can be obtained simultaneously, if desired). If a plot is desired of any or all of the spectra, the user supplies the full scale value required. A summation of any region of any of the three spectra may also be obtained.

```

C   SPECTRA STRIPPING PROGRAM
    DIMENSION IAC(128), IRC(128), IC(128), ID(128), IG(128), IH(128), IARY(51)
    WRITE(6,999)
999  FORMAT(3H G0)
    1  FORMAT(2X, I3)
    3  FORMAT(7(I6, 2X), I6)
    7  FORMAT(I6)
    DO 2 I=1, 128, 8
    2  READ(5, 3) IAC(I), IAC(I+1), IAC(I+2), IAC(I+3), IAC(I+4), IAC(I+5),
    IAC(I+6), IAC(I+7)
    DO 777 K=1, 128, 8
    777  WRITE(6, 3) IACK), IACK+1), IACK+2), IACK+3), IACK+4), IACK+5),
    IACK+6), IACK+7)
    WRITE(6, 100)
    100 FORMAT(18H TAPE OK, >0, N0T, <0)
    READ(5, 1) ICORR
C   IF ICORR <=, 0 CORRECT TAPE
    IF(ICORR) 4, 4, 5
    4  WRITE(6, 6)
    6  FORMAT( 17H TYPE CHANNEL NO.)
    READ(5, 1) ICA
    WRITE(6, 7) IAC(ICA)
    READ(5, 7) IAC(ICA)
    WRITE(6, 7) IAC(ICA)
    WRITE(6, 101)
    101 FORMAT(12H MORE<0, OK>0)
    READ(5, 1) IC0NT
C   IF IC0NT <=, 0 CORRECT MORE
    IF(IC0NT) 4, 4, 5
    5  WRITE(6, 102)
    102 FORMAT(20H 2ND TAPE<0; 1 ONLY>0)
    READ(5, 1) NT
C   IF NT <=, 0 2ND TAPE
    IF(NT) 8, 8, 9
    8  DO 10 I=1, 128, 8
    10  READ(5, 3) IRC(I), IRC(I+1), IRC(I+2), IRC(I+3), IRC(I+4), IRC(I+5),
    IRC(I+6), IRC(I+7)
    DO 690 J9=1, 128, 8
    690  WRITE(6, 3) IRC(J9), IRC(J9+1), IRC(J9+2), IRC(J9+3), IRC(J9+4),
    IRC(J9+5), IRC(J9+6), IRC(J9+7)
    WRITE(6, 100)
    READ(5, 1) ICORR
    IF(ICORR) 11, 11, 12
    11  WRITE(6, 6)
    READ(5, 1) ICB
    WRITE(6, 7) IRC(ICB)
    READ(5, 7) IRC(ICB)
    WRITE(6, 7) IRC(ICB)
    WRITE(6, 101)

```

```

      READ(5,1)ICONT
      IF(ICONT)11,11,12
12  WRITE(6,103)
103  FORMAT(14H A-P=<0;P-A=>0)
      READ(5,1)ISUB
      WRITE(6,230)
230  FORMAT(2X,26H WRITE NORMALIZATION CONST)
      READ(5,232)CORFAC
232  FORMAT(2X,F6.3)
      IF(ISUB)13,13,14
13  DO 15 I2=1,128
      IC(I2)=IA(I2)-IB(I2)*CORFAC
      IF(IC(I2))16,15,15
16  IC(I2)=0
15  CONTINUE
      GO TO 14
14  DO 17 I3=1,128
      IC(I3)=IP(I3)-IA(I3)*CORFAC
      IF(IC(I3))18,17,17
18  IC(I3)=0
17  CONTINUE
69  CONTINUE
      WRITE(6,104)
104  FORMAT(12H A=1, F=2, C=3)
      READ(5,1)IWT
C      A=1; F=2; C=3
      IF(IWT-2)9,29,19
19  DO 20 I4=1,128,8
20  WRITE(6,3)IC(I4),IC(I4+1),IC(I4+2),IC(I4+3),IC(I4+4),
1,IC(I4+5),IC(I4+6),IC(I4+7)
      GO TO 40
29  DO 30 I5=1,128,8
30  WRITE(6,3)IB(I5),IB(I5+1),IB(I5+2),IB(I5+3),IB(I5+4),
1IB(I5+5),IB(I5+6),IB(I5+7)
      GO TO 40
9   DO 22 I6=1,128,8
22  WRITE(6,3)IA(I6),IA(I6+1),IA(I6+2),IA(I6+3),IA(I6+4),
1IA(I6+5),IA(I6+6),IA(I6+7)
40  CONTINUE
      WRITE(6,41)
41  FORMAT(26H ANOTHER TAPE, Y=POS, N0=NEG)
      READ(5,1)ITP
      IF(ITP)23,23,69
23  CONTINUE
      WRITE(6,601)
601  FORMAT(1X,' DO YOU WANT A PLOT; Y>0, N<0')
      READ(5,1)IQ
      IF(IQ)602,602,603
603  WRITE(6,604)

```

```

604 FORMAT(IX, ' WHICH TAPE; A=1, B=2, C=3')
   READ(6, 1)INS
   IF(INS-2)605, 607, 609
605 D0 606 IXX=1, 128
606 IH(IXX)=IA(IXX)
   GO TO 611
607 D0 608 IXY=1, 128
608 IH(IXY)=IR(IXY)
   GO TO 611
609 D0 610 IXZ=1, 128
610 IH(IXZ)=IC(IXZ)
611 WRITE(6, 612)
612 FORMAT(IX, ' WRITE LARGEST VALUE')
   READ(5, 7)ICAL
   CAL=ICAL/50
   D0 613 IT=1, 128
   IG(IT)=INT(IH(IT)/CAL)+1
   IF(IG(IT)-51)613, 613, 713
713 IG(IT)=51
613 CONTINUE
   D0 618 IS=1, 128
   D0 616 IP=1, 51
   IF(IP-IG(IS))614, 615, 614
614 IAFY(IP)=' '
   GO TO 616
615 IAFY(IP)='*'
616 CONTINUE
   WRITE(6, 617)IS, IAFY
617 FORMAT(IX, I3, T5, S1A1)
618 CONTINUE
   WRITE(6, 718)
718 FORMAT(2X, ' DO YOU WANT ANOTHER PLOT; Y<0, N>0')
   READ(5, 1)KK
   IF(KK)602, 603, 602
602 WRITE(6, 105)
105 FORMAT(29H D0 YOU WANT A SIM+Y=>0; N=<0)
   READ(5, 1)JS
   IF(JS)24, 24, 26
26 WRITE(6, 106)
106 FORMAT(25H WRITE CH. START; CH. STOP)
   READ(5, 107)KST, KSP
107 FORMAT(2X, I3, 2X, I3)
   WRITE(6, 108)
108 FORMAT(11H WHICH TAPE)
   READ(5, 1)LS
   IF(LS-2)70, 80, 90
70 D0 71 LA=1, 128
71 ID(LA)=IA(LA)
   GO TO 200

```

```
80  D0 81 LP=1,128
81  ID(LP)=IP(LP)
    GO TO 200
90  D0 91 LC=1,128
91  ID(LC)=IC(LC)
    GO TO 200
200  ISIM=0
    D0 201 MS=K ST,K SP
201  ISIM=ISIM+ID(MS)
    WRITE(6,202) ISIM
202  FORMAT(6H ISIM=,I8)
    GO TO 23
24  STOP
    END
```

00

REFERENCES

1. W. Bambynek, B. Crasemann, R. W. Fink, H. U. Freund, H. Mark, C. D. Swift, R. E. Price, and P. V. Rao, Reviews of Modern Physics (to be published).
2. E. Karttunen, H. U. Freund, and R. W. Fink, Nuclear Physics A131, 343(1969).
3. H. H. Grother, J. W. Hammer, and K. W. Hoffmann, Zeitschrift fur Physik 225, 293(1969).
4. H. T. Easterday and R. L. Smith, Nucl. Phys. 20, 155(1960).
5. T. Paradellis and S. Hontzeas, Nucl. Phys. A131, 378(1969).
6. D. E. Raeside, M. A. Luding, J. J. Reidy, and M. L. Wiedenbeck, Nucl. Phys. A130, 677(1969).
7. P. V. Rao, D. K. McDaniels, and B. Crasemann, Nucl. Phys. 81, 296(1966).
8. D. K. Berkey, Physical Review 45, 437(1934).
9. J. Pahor, A. Kodre, and A. Moljk, Z. Physik (to be published).
10. E. Karttunen, PhD Dissertation, Georgia Institute of Technology, 1971.
11. a) H. U. Freund, H. Genz, J. B. Sieberts, and R. W. Fink, Nucl. Phys. A138, 200(1969)
b) J. Scobie, R. B. Moler, and R. W. Fink, Phys. Rev. 116, 657(1959).
12. J. N. Bahcall, Phys. Rev. 132, 362(1963).
13. B. L. Robinson, Nucl. Phys. 64, 197(1965).
14. C. M. Lederer, J. M. Hollander, and I. Perlman, Table of Isotopes, John Wiley and Sons Inc. New York, 1968.
15. H. Genz, PhD Dissertation, Emory University, 1971; and J. G. Pengra, H. Genz, J.P. Renier, and R. W. Fink, Phys. Rev. C(in Press).

REFERENCES (Concluded)

16. E. J. McGuire, Phys. Rev. A2, 273(1970).
17. E. J. Kostroun, M. H. Chen, B. Crasemann, Phys. Rev. A3, 533(1971).
18. D. L. Walters and C. P. Bhalla, Phys. Rev. A3, 1919(1971).
19. J. Pahore, A. Kodre, and A. Moljk, Z Physik, 230, 287(1970).
20. G. Winter, Nucl. Phys. A113, 617(1968).
21. H. Behrens, J. Jänecke, Landolt-Börnstein New Series, I/4.
22. M. J. Martin, P. H. Blichert-Poft, Nuclear Data Tables, A8, 1(1970).
23. L. N. Zyryanova and Yu. P. Suslov, Proceedings of the Conference on Electron Capture, Debrecen, Hungary, 1968, p.45.
24. R. E. Watson and A. J. Freeman, Phys. Rev. 123, 521(1961).
25. J. N. Bahcall, Phys. Rev. 132, 362(1963).
26. Yu. P. Suslov, Bulletin of the Academy of Science USSR, 34, 91(1970).
27. E. Vatai, Nucl. Phys. A156, 541(1970).